Remote Sensing of Environment 311 (2024) 114276

Contents lists available at ScienceDirect

Remote Sensing of Environment

journal homepage: www.elsevier.com/locate/rse

Intercomparison of global foliar trait maps reveals fundamental differences and limitations of upscaling approaches

Benjamin Dechant [a,b,*], Jens Kattge [c,a], Ryan Pavlick [d], Fabian D. Schneider [d], Francesco M. Sabatini [e,f], Álvaro Moreno-Martínez [g], Ethan E. Butler [h], Peter M. van Bodegom [i], Helena Vallicrosa [j,k,l], Teja Kattenborn [m,a], Coline C.F. Boonman [n], Nima Madani [o,d], Ian J. Wright [p,q], Ning Dong [r,s], Hannes Feilhauer [t,a], Josep Peñuelas [k,l], Jordi Sardans [k,l], Jesús Aguirre-Gutiérrez [u,v], Peter B. Reich [w,h,p], Pedro J. Leitão [t,a], Jeannine Cavender-Bares [x], Isla H. Myers-Smith [y], Sandra M. Durán [z], Holly Croft [aa], I. Colin Prentice [r,ab], Andreas Huth [ac,ad,a], Karin Rebel [ae], Sönke Zaehle [c], Irena Šímová [af,ag], Sandra Díaz [ah,ai], Markus Reichstein [c,a], Christopher Schiller [aj], Helge Bruelheide [ak,a], Miguel Mahecha [t,a], Christian Wirth [al,c], Yadvinder Malhi [u,v], Philip A. Townsend [d,am]

[a] German Centre for Integrative Biodiversity Research (iDiv) Halle-Jena-Leipzig, Puschstr. 4, D-04103 Leipzig, Germany
[b] Leipzig University, Ritterstraße 26, 04109 Leipzig, Germany
[c] Max Planck Institute for Biogeochemistry, Hans Knöll Str. 10, 07745 Jena, Germany
[d] Jet Propulsion Laboratory, California Institute of Technology, 4800 Oak Grove Drive, Pasadena, CA 91109, USA
[e] BIOME Lab, Department of Biological, Geological and Environmental Sciences (BiGeA), Alma Mater Studiorum University of Bologna, Via Irnerio 42, Bologna 40126, Italy
[f] Czech University of Life Sciences Prague, Faculty of Forestry and Wood Sciences, Kamýcká 129, 165 21 Praha Suchdol, Czech Republic
[g] Image Processing Laboratory (IPL), Universitat de València, Valencia, Spain
[h] Department of Forest Resources, University of Minnesota, 1530 Cleveland Ave N, St. Paul, MN 55108, United States of America
[i] Institute of Environmental Sciences, Leiden University, Einsteinweg 2, 2333 CC Leiden, the Netherlands
[j] Department of Civil and Environmental Engineering, Massachusetts Institute of Technology, Cambridge, MA, USA
[k] CSIC, Global Ecology Unit CREAF-CSIC-UAB, Bellaterra, Barcelona 08913, Catalonia, Spain
[l] CREAF, 08913 Cerdanyola del Vallès, Barcelona 08913, Catalonia, Spain
[m] Department for Sensor-based Geoinformatics, Faculty of Environment and Natural Resources, University of Freiburg, Germany
[n] Center for Biodiversity Dynamics in a Changing World (BIOCHANGE) and Section for Ecoinformatics & Biodiversity, Department of Biology, Aarhus University, Ny Munkegade 114, 8000 Aarhus C, Denmark
[o] UCLA Joint Institute for Regional Earth System Science and Engineering, 4242 Young Hall, 607 Charles E. Young Drive East, Los Angeles, CA 90095, USA
[p] Hawkesbury Institute for the Environment, Western Sydney University, Locked Bag 1797, Penrith, NSW 2751, Australia
[q] School of Natural Sciences, Macquarie University, NSW 2109, Australia
[r] Georgina Mace Centre for the Living Planet, Department of Life Sciences, Imperial College London, Silwood Park Campus, Buckhurst Road, Ascot SL5 7PY, UK
[s] Department of Biological Sciences, Macquarie University, North Ryde, NSW 2109, Australia
[t] Remote Sensing Centre for Earth System Research (RSC4Earth), Leipzig University and Helmholtz Centre for Environmental Research, Talstr. 35, 04103 Leipzig, Germany
[u] Environmental Change Institute, School of Geography and the Environment, University of Oxford, Oxford, UK
[v] Leverhulme Centre for Nature Recovery, University of Oxford, Oxford OX13QY, UK
[w] Institute for Global Change Biology, School for the Environment and Sustainability, University of Michigan, Ann Arbor, MI 48109, United States
[x] Department of Ecology, Evolution and Behavior, University of Minnesota, 1479 Gortner Ave., Saint Paul, MN 55108, United States of America
[y] School of GeoSciences, University of Edinburgh, Edinburgh EH9 3FF, UK
[z] Department of Forest and Rangeland Stewardship, Colorado State University, Fort Collins, CO, USA
[aa] School of Biosciences, University of Sheffield, Sheffield S10 2TN, UK
[ab] Ministry of Education Key Laboratory for Earth System Modeling, Department of Earth System Science, Tsinghua University, Beijing 100084, China
[ac] Helmholtz Centre for Environmental Research - UFZ, Permoserstr. 15, 04318 Leipzig, Germany
[ad] University of Osnabrück, Barbarastraße 12, 49076 Osnabrück, Germany
[ae] Copernicus Institute of Sustainable Development, Environmental Sciences, Faculty of Geosciences, Utrecht University, Utrecht, the Netherlands
[af] Center for Theoretical Study, Charles University, Husova 4, 110 00 Prague, Czech Republic
[ag] Department of Ecology, Faculty of Science, Charles University, Viničná 7, 128 44 Prague, Czech Republic
[ah] Consejo Nacional de investigaciones Científcas y Técnicas, Instituto Multidisciplinario de Biología Vegetal (IMBIV), Córdoba, Argentina

* Corresponding author at: German Centre for Integrative Biodiversity Research (iDiv) Halle-Jena-Leipzig, Puschstr. 4, D-04103 Leipzig, Germany.
E-mail address: benjamin.dechant@idiv.de (B. Dechant).

https://doi.org/10.1016/j.rse.2024.114276
Received 5 December 2023; Received in revised form 25 May 2024; Accepted 15 June 2024
Available online 27 June 2024

[ai] Facultad de Ciencias Exactas, Físicas y Naturales, Universidad Nacional de Córdoba, Casilla de Correo 495, 4000 Córdoba, Argentina
[aj] Institute of Geographical Sciences, Free University Berlin, Malteserstraße 74-100, 12249 Berlin, Germany
[ak] Institute of Biology/Geobotany and Botanical Garden, Martin Luther University Halle-Wittenberg, Am Kirchtor 1, 06108 Halle, Germany
[al] Institute of Systematic Botany and Functional Biodiversity, Leipzig University, Leipzig, Germany
[am] University of Wisconsin, Madison, WI, USA

ARTICLE INFO

Editor: Jing M. Chen

Keywords:
Foliar trait
Specific leaf area
Leaf nitrogen
Leaf phosphorus
Global map
Upscaling

ABSTRACT

Foliar traits such as specific leaf area (SLA), leaf nitrogen (N), and phosphorus (P) concentrations play important roles in plant economic strategies and ecosystem functioning. Various global maps of these foliar traits have been generated using statistical upscaling approaches based on in-situ trait observations. Here, we intercompare such global upscaled foliar trait maps at 0.5° spatial resolution (six maps for SLA, five for N, three for P), categorize the upscaling approaches used to generate them, and evaluate the maps with trait estimates from a global database of vegetation plots (sPlotOpen). We disentangled the contributions from different plant functional types (PFTs) to the upscaled maps and quantified the impacts of using different plot-level trait metrics on the evaluation with sPlotOpen: community weighted mean (CWM) and top-of-canopy weighted mean (TWM). We found that the global foliar trait maps of SLA and N differ drastically and fall into two groups that are almost uncorrelated (for P only maps from one group were available). The primary factor explaining the differences between these groups is the use of PFT information combined with remote sensing-derived land cover products in one group while the other group mostly relied on environmental predictors alone. The maps that used PFT and corresponding land cover information exhibit considerable similarities in spatial patterns that are strongly driven by land cover. The maps not using PFTs show a lower level of similarity and tend to be strongly driven by individual environmental variables. Upscaled maps of both groups were moderately correlated to sPlotOpen data aggregated to the grid-cell level ($R = 0.2$–0.6) when processing sPlotOpen in a way that is consistent with the respective trait upscaling approaches, including the plot-level trait metric (CWM or TWM) and the scaling to the grid cells with or without accounting for fractional land cover. The impact of using TWM or CWM was relevant, but considerably smaller than that of the PFT and land cover information. The maps using PFT and land cover information better reproduce the between-PFT trait differences of sPlotOpen data, while the two groups performed similarly in capturing within-PFT trait variation.

Our findings highlight the importance of explicitly accounting for within-grid-cell trait variation, which has important implications for applications using existing maps and future upscaling efforts. Remote sensing information has great potential to reduce uncertainties related to scaling from in-situ observations to grid cells and the regression-based mapping steps involved in the upscaling.

1. Introduction

Vascular plants play a crucial role in the terrestrial Earth system due to their exchange of carbon, water, nutrients, and energy with the atmosphere and the pedosphere. Moreover, plants are important elements in the biosphere as they are strong drivers of the population dynamics of other organisms. Functional traits are important for characterizing vegetation function and plant ecological strategies related to metrics of performance, such as nutrient retention, biomass accumulation and CO_2 uptake (Bongers et al., 2021; Díaz et al., 2016; Wright et al., 2004). In particular, morphological and chemical leaf traits, such as specific leaf area (SLA) and leaf concentrations of phosphorus (P) and nitrogen (N), are key components of the leaf economic spectrum (Wright et al., 2004). In turn, the leaf economic spectrum contributes to determining plant growth strategies and canopy carbon exchange dynamics globally (Reich, 2014).

Due to their important roles in plant metabolism, the leaf traits N, P and SLA have been used as inputs to land surface models (Walker et al., 2017), but often in highly simplified ways. This is due to the challenges of estimating these traits robustly at the global scale using currently available remote sensing methods due to their weaker light absorption signals compared to leaf chlorophyll content for which global maps already exist (Croft et al., 2020; Wan et al., 2024; Xu et al., 2022). Therefore, many land surface modeling applications have been using plant functional type (PFT) look-up tables for key traits such as photosynthetic capacity, which is closely related with N, P and SLA (Kattge et al., 2009; Walker et al., 2014). These look-up tables contain PFT mean trait values that can be combined with remote sensing-based maps of land-cover types dominated by particular PFTs to approximate global trait distributions, but these approaches ignore large within-PFT trait variability driven by inter- and intraspecific trait variation (Kattge et al., 2011; Scheiter et al., 2013; Van Bodegom et al., 2012). Furthermore, representing land cover types by only their dominant PFTs emphasizes top-of-canopy vegetation and ignores the complexity of multi-layered ecosystems.

To overcome the limitations of simplified approaches based on PFT mean trait values for land surface modeling applications and to address ecological questions e.g. related to aspects of functional biodiversity, static maps of SLA, N, P and other traits have been produced based on in-situ, leaf-level trait measurements using statistical upscaling approaches at regional (Loozen et al., 2020; Šímová et al., 2018; Swenson and Weiser, 2010; Zhang et al., 2021) and global scales (Boonman et al., 2020; Butler et al., 2017; Madani et al., 2018; Moreno-Martínez et al., 2018; Schiller et al., 2021; Vallicrosa et al., 2022; van Bodegom et al., 2014; Wolf et al., 2022). These upscaled maps of N, P and SLA were generated using different methods, different trait databases and were developed for a range of purposes, such as supporting land surface modeling, biodiversity characterization or a trait-based estimation of the distribution of vegetation types. Given these contrasting approaches and aims, we sought to understand the degree of consistency among these maps, as well as their performance when evaluated in comparison to plot level in-situ data.

For potential users, the reliability of upscaled global foliar trait maps and their suitability for specific purposes are difficult to assess. Identifying the key sources of uncertainties and limitations of these maps can provide guidance for users and help improve the global mapping of plant traits. Here, we provide a comprehensive evaluation of the current global upscaled foliar trait maps of SLA, N, P consisting of the following elements:

1) Categorization of upscaling approaches;
2) Comparison of spatial patterns and attribution of differences to upscaling methodology;

3) Evaluation against trait estimates based on a global vegetation plot database.

2. Materials and methods

2.1. Terminology

The upscaling of foliar trait maps is relevant for different scientific communities (e.g., land surface modeling, vegetation remote sensing, macroecology), which may use different or partly similar terms with different meanings. To avoid misunderstandings and be able to use convenient shorthand notations for concepts frequently used throughout the manuscript, we clarify our use of key terms with the following definitions (Table 1). We do not claim that these definitions are necessarily optimal or universal, rather, they serve as a pragmatic way to clarify terms used in the presentation of our study. Note that the land cover types (LCTs) we consider are land cover *functional* types that can be directly matched to PFTs (Table 1) in the sense used in previous work (Friedl et al., 2002; Poulter et al., 2015). We use the more general term 'PFT information' to include both (in-situ) PFT and (grid-cell-level) LCT for the sake of convenience as PFT and LCT data were typically used together in the upscaling.

2.2. Trait maps

We identified seven publications in the literature (state June 2022) that present global, statistically upscaled trait maps with at least one of the three traits SLA, N or P: van Bodegom et al. (2014); Butler et al. (2017); Madani et al. (2018), Moreno-Martínez et al. (2018), Boonman et al. (2020), Schiller et al. (2021), and Vallicrosa et al. (2022) (Table 2). For the sake of simplicity, we use a short version of the last name of the first author of each map-related publication to refer to the different maps, e.g., 'Bodegom' refers to the map of van Bodegom et al. (2014). 'Moreno' refers to Moreno-Martínez et al. (2018) (see Table 2).

The degree of completeness of the spatial coverage of the maps differed. Four maps provided gap-free global maps (Bodegom, Butler, Madani, Boonman), while the two high-resolution maps excluded cropland (Moreno, Vallicrosa). Schiller had gaps in different regions due to the availability/selection of plant photographs from iNaturalist. All upscaling approaches except Madani only considered trait variation in natural vegetation and excluded foliar traits in croplands. This implies that trait values in cropland areas indicate traits of natural vegetation actually or potentially occurring there. While most approaches considered vegetation of different growth forms, Vallicrosa only mapped traits for woody vegetation (Table 2).

Table 1
Glossary of terms.

Plant functional type (PFT)	classification of plants, mostly based on growth form, leaf type and leaf phenology. Example: evergreen needleleaf tree.
Land cover type (LCT)	remote sensing-based classification of the land cover, dominated by specific PFTs. Example: evergreen needleleaf forest.
Community weighted mean (CWM)	the mean trait value of a community weighted by the species cover, abundance, or biomass. In the case of the sPlotOpen dataset the weighting is done by species cover or abundance.
Top-of-canopy weighted mean (TWM)	the mean trait value at the top-of-canopy weighted by the cover of the species that constitute the dominant PFT of a plot.
Homogeneous grid cells	grid cells with low trait variability, either occupied by a single LCT or several LCTs with similar trait values.
Heterogeneous grid cells	grid cells with high trait variability, occupied by more than one dominant PFT with notable differences in mean trait values of the dominant PFTs.

Table 2
Overview of the upscaling approaches and the corresponding maps. Note that PFT use also implies use of land cover type products.

Lead author	Year	Traits	PFT use	Resolution[†]	Vegetation Considered	Reference
Bodegom	2014	SLA	no	0.5 °	Natural[‡]	van Bodegom et al. (2014)
Butler	2017	SLA, N, P	yes	0.5 °	Natural[‡]	Butler et al. (2017)
Madani	2018	SLA	yes	0.05 °	All	Madani et al. (2018)
Moreno	2018	SLA, N, P	yes	0.008°	Natural[*]	Moreno-Martínez et al. (2018)
Boonman	2020	SLA, N, P	no	0.5 °	Natural[‡]	Boonman et al. (2020)
Vallicrosa	2021	N, P	yes	0.008°	Woody	Vallicrosa et al. (2022)
Schiller	2021	SLA, N	no	0.5 °	Natural[‡]	Schiller et al. (2021)

[†] The resolutions 0.5°, 0.05°, and 0.008° correspond to square grid cell sizes of about 50 km, 5 km and 1 km at the equator.
[‡] No crop traits in training data but predictions for cropland areas, corresponding to potential natural vegetation.
[*] No crop traits in training data and no predictions for cropland areas.

2.3. Upscaling approaches

All approaches derived gridded global trait maps from globally distributed leaf-level in-situ observations (Fig. S1) and can be characterized by two steps of upscaling: (1) leaf-to-grid scaling, i.e. the scaling of in-situ leaf-level data to the respective cells of a spatial grid, and (2) spatialization, i.e., increasing the spatial coverage from the limited number of grid cells with in-situ data to the global land surface (Fig. 1). All approaches except Schiller applied step (1) before step (2) (Fig. 1) and applied regression-based spatialization that first established trait-environment relationships for the reference grid cells and then applied them to the global vegetated land surface to obtain global maps. Schiller, however, switched the order of the two upscaling steps and first estimated trait values for a large number of iNaturalist photographs of individual plants distributed globally and aggregated these trait values to grid-cell-level in the second step.

There were important differences between the upscaling approaches in essentially all aspects of the upscaling processing chain (Fig. 1). The approaches differed in their motivations, input data and its processing, leaf-to-grid scaling methods, and spatialization, including both the choice of predictor variables and regression algorithms (Fig. 1, Text S1 in the supplementary material). The only study that calculated local community mean trait values from the in-situ data before grid-cell level aggregation was Boonman, the other studies averaged all available in-situ observations within a grid cell either pooled (van Bodegom) or separately per PFT (Madani, Moreno, Vallicrosa). The environmental predictors used in the upscaling approaches were mainly related to temperature, solar radiation, water availability and soil characteristics (Table S1) and came from a variety of climate and soil products (Table S2). Importantly, there were differences whether and how PFT and remote sensing derived LCT information was used for upscaling (Fig. 1). Moreno was the only approach that directly used optical reflectance satellite remote sensing data as predictors in the spatialization (Table S1).

2.3.1. Categorization of upscaling strategies

All maps used environmental predictor information ('Env') in the spatialization step, but only some used PFT information. Therefore, we use the shorthand notation of 'PFT + Env' vs. 'Env' maps to more generally distinguish the upscaling approaches that used PFT information from those that did not. Note that there are considerable differences in the way PFT information was used in the PFT + Env approaches, e.g.

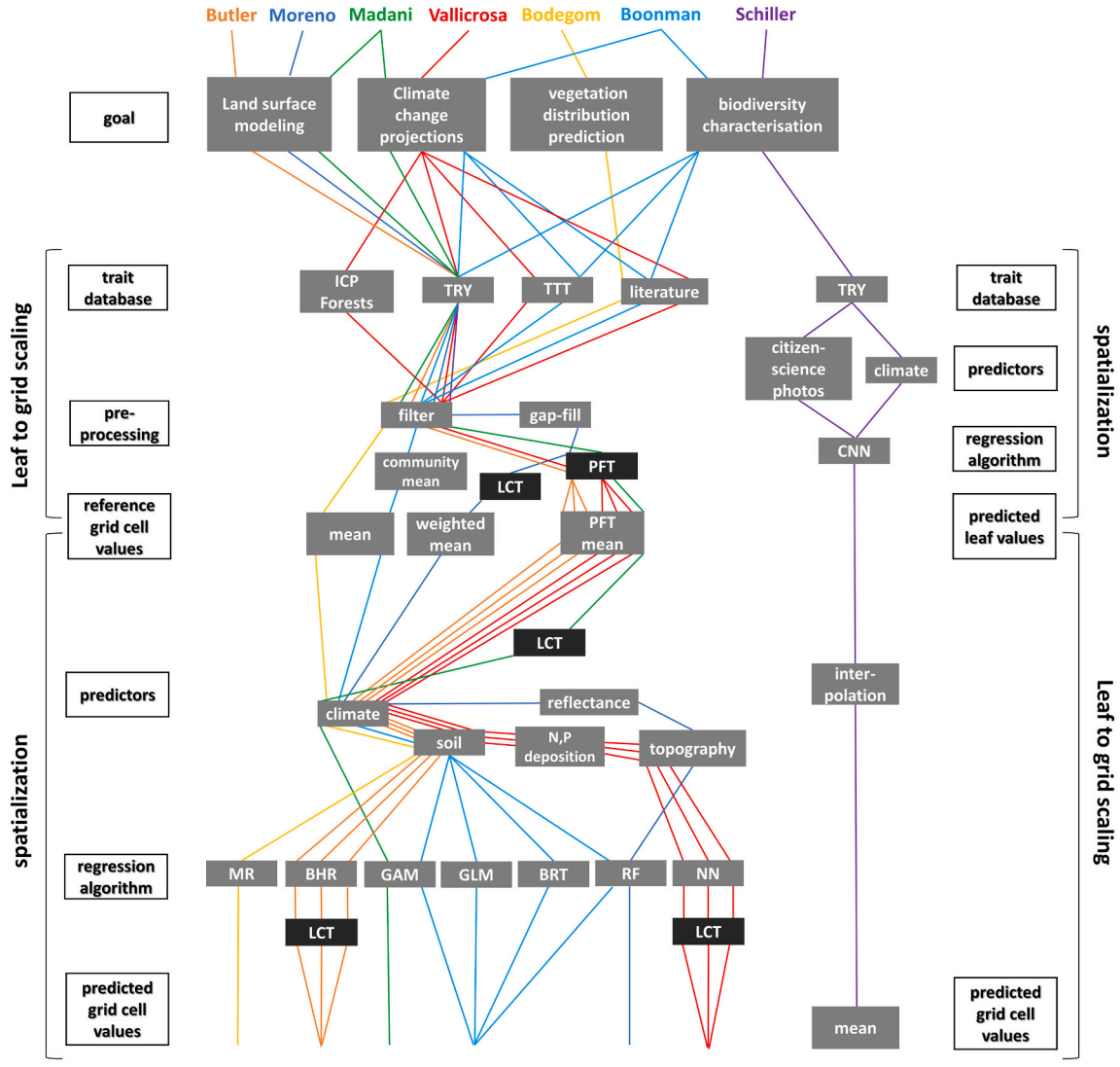

Fig. 1. Schematic overview of the upscaling approaches. Each upscaling approach is shown in a separate color. Special emphasis is put on the use of plant functional type (PFT) and land cover type (LCT) information shown in dark gray color. The explanatory column on the left hand side applies to all approaches except Schiller for which the corresponding column on the right hand side applies. 'TTT' refers to the Tundra Trait Team database, 'literature' to data based on individual publications. The regression algorithms include multiple linear regression (MR), Bayesian hierarchical regression (BHR), generalized additive models (GAM), generalized linear models (GLM), generalized boosted models (GBM), random forests (RF), neural networks (NN), convolutional neural networks (CNN).

Moreno used PFTs only in the first step of the upscaling, while Butler only used it at the end of the second step (Fig. 1). Also, the Schiller map is categorized as 'Env' upscaling approach for the sake of convenience (Fig. 1), although information from ground-based RGB images was used in addition to environmental drivers.

2.3.2. *Additional versions of the Butler and Moreno maps*

To quantify the relative contributions of different types of predictor information to the upscaled trait maps, we also analyzed versions of the Butler and Moreno trait maps that differed only in the predictor variables used. Note that the PFT maps only using fixed trait values per LCT are referred to as categorical maps in Butler et al. (2017). We also make use of this term (categorical) in the text to avoid potential confusion of PFT trait maps with maps of PFT cover that would correspond to LCT maps. We adjusted the mean trait values per LCT of the categorical Butler maps to better capture the trait patters of the PFT + Env upscaled Butler maps (Fig. S2).

2.4. *Data processing*

2.4.1. *Global foliar trait maps*

We used global trait maps provided by the map developers (the leading authors of the relevant publications) to ensure that we had the most up-to-date and correct versions of the upscaling products. Links to access the maps are provided in the supplementary material (Table S3). We only used maps representing the present and recent past and did not consider maps of future change predictions such as Madani et al. (2018). We aggregated the higher resolution maps (Madani, Moreno, Vallicrosa) to the common resolution of 0.5° using the Bodegom map as reference regarding the projection and coordinate origin. For this, we used the *aggregate* function of the *raster* package in R (Hijmans, 2022) and averaged over all available high resolution grid cells within a coarse grid cell ignoring missing-data and zero values. Non-vegetated grid cells such as bare soil, ice/snow etc. were excluded by selecting grid cells with a minimum vegetation cover of of 5% based on the LCT map used by Butler. Madani was the only data set to provide estimates for croplands, so prior to aggregating to 0.5°, we masked out the cropland grid cells at the original resolution of 0.05° based on the land cover map used by

Madani. We did not mask out cropland-dominated grid cells at 0.5° to include the trait variation of (potential) natural vegetation in cropland regions.

2.4.2. Separation of land cover - driven and environmentally driven trait variation and stratification by PFT

Our initial analyses revealed that LCT-driven trait variation dominated the global spatial trait patterns of the PFT + Env maps. As one objective of the upscaling approaches was estimating trait variation within PFTs, it is important to disentang,le the dominant LCT-driven trait variation that is related to *between*-PFT trait variation from the variation *within* PFTs. The common approach to quantify variations within LCTs is to select only homogeneous grid cells by applying a threshold on the cover fractions of LCTs. However, this approach has an important limitation: the land cover threshold only considers the homogeneity in land cover but not the variation of foliar traits, which we aim to quantify. Therefore, we estimated the trait heterogeneity based on fractional LCT using PFT mean trait values. We found that the relationship between land cover homogeneity and trait homogeneity can be complex, partly showing even a strong negative relationship (Figs. 2, S3).

This implies that in addition to a threshold on the cover fraction of LCTs, a second threshold on the homogeneity in traits is needed. This double threshold approach ('trait heterogeneity filtering'), resulted in a reasonable number of homogeneous grid cells for three of the six LCTs, but for the remaining three LCTs not enough grid cells remain (Figs. S2c). Therefore, we developed a complementary second approach to unmix LCTs in heterogeneous grid cells (Text S2, Figs. S3, S4). For analyses at the level of PFTs/LCTs we combined the two approaches to obtain sufficient data for all LCTs. Both approaches are described in detail in supplementary Text S2. Deciduous needleleaf forest (DNF) was excluded from further analyses due to the sparseness of in-situ reference data and the limited geographic extent of the distribution compared to the other LCTs: evergreen broadleaf forest (EBF), evergreen needleleaf forest (ENF), deciduous broadleaf forest (DBF), shrubland (SHR) and grassland (GRA).

2.4.3. Evaluation against sPlotOpen

To evaluate the upscaled maps against data not directly used in the upscaling, we used the sPlotOpen database (Sabatini et al., 2021). sPlotOpen is an open-access collection of 95,104 vegetation plots sampled in the field, spanning 114 countries. It consists of a stratified random selection of vegetation plots derived from sPlot - The Global Vegetation plot database (Bruelheide et al., 2019). Plots vary widely in size, ranging between 0.03 and 40,000 m^2. For each plot, sPlotOpen reports the list of vascular plant species, together with a measure of their relative abundance. Species mean trait values, as extracted from the TRY database (Kattge et al., 2020, 2011), were combined with species abundance data to calculate plot-level community weighted mean (CWM) trait values. To evaluate the impact of vertical variations of foliar traits due to species composition, we calculated top-of-canopy weight mean (TWM) trait estimates per plot, in addition to the standard CWM trait estimates, which integrate traits from all vegetation layers. This was done by first determining the dominant PFT of each plot using thresholds on the species cover of a given PFT (Table S4) and then calculating the weighted mean over all species of the dominant PFT of the plot. One motivation for conducting the CWM vs. TWM comparison was the differences in upscaling approaches regarding the scaling from the leaf to the grid cell. To compare sPlotOpen and upscaled maps at the level of individual PFTs, we stratified both CWM and TWM by PFT by using the dominant PFT of the plot. We used the six PFT categories defined above (ENF, DNF, EBF, DBF, SHR, GRA) and matched the species in sPlotOpen to these categories using plant growth form, leaf type and leaf phenology type from the TRY database and literature.

We compared characteristics of the upscaled maps with sPlotOpen at two levels: using *plot*-level sPlotOpen data and *grid-cell*-level sPlotOpen data.

Using *grid-cell-level* sPlotOpen data enables a more direct comparison to upscaled maps than using plot-level data, but for this the sPlotOpen plot data has to be scaled to the grid cell given the fact that sPlotOpen plots are much smaller than the typical grid cell size (50 × 50 km) of global upscaled trait maps. This scaling was done as follows to ensure direct comparability to the upscaled maps. For the comparison to Env upscaled maps, we aggregated the plot-level CWMs to the 0.5° grid cells without any weighting. For the comparison to PFT + Env upscaled maps, for each PFT, we first aggregated the plot-level TWM data to the 0.5° grid cells without weighting and then combined the six sPlotOpen PFT maps per trait by applying a weighted average based on the fractional land cover for each 0.5° grid cell. Data filtering was applied to ensure that sufficient data from sPlotOpen was available to be reasonably representative of a grid cell by applying a 99% threshold on the cumulated land cover. The high threshold is necessary as small fractions of missing coverage can considerably impact the result if the missing PFT has a very different trait value compared to the other PFTs that are represented, e.g. ENF (Fig. 2). Also, outliers in the sPlotOpen data were removed by applying a 90th percentile threshold for each trait. For the comparison of between- and within-PFT trait variation we used unweighted grid-cell averages of all relevant plots per PFT.

2.5. Statistical analyses

Principal component analysis (PCA) was used to visualize the grouping and relative correlation of different trait maps. Variables were centered and scaled to unit variance for PCA using the *prcomp* function in base R. Pearson correlation (R) was used to quantify the similarity between two given maps. Apart from the 'normal' correlation based on all selected grid cells, we also quantified the degree of 'local correlation' by calculating correlations in a moving window of 3 × 3 grid cells to quantify the similarity in spatial patterns at smaller scales using the *corLocal* function of the *raster* package (Hijmans, 2022). For each pair of

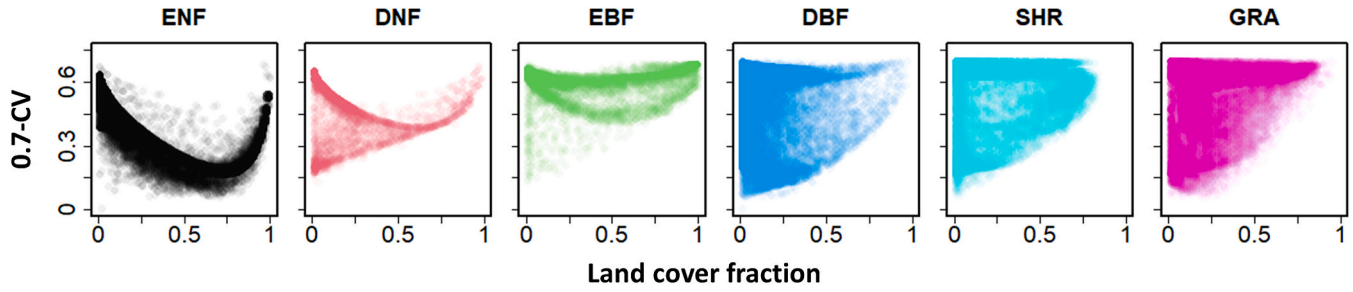

Fig. 2. Relationships between land cover homogeneityand foliar trait homogeneity for the example of specific leaf area (SLA). The within-grid cell coefficient of variation (CV) of SLA is shown as indicator of trait heterogeneity. The CV was estimated from land cover fractions and plant functional type (PFT)-specific trait values. The relationship between fcov and 0.7-CV as indicator of trait homogeneity is shown per land cover type (ENF: evergreen needleleaf forest; DNF: deciduous needleleaf forest; EBF: evergreen broadleaf forest; DBF: deciduous broadleaf forest; SHR: shrubland; GRA: grassland).

maps, the local correlation produces a correlation map and to summarize that map, the median was calculated.

All analyses and image processing were conducted using R version 4.0.2 (R Core Team, 2012), primarily with the *raster* package (Hijmans, 2022).

3. Results

3.1. Intercomparison of global maps and attribution of differences

3.1.1. Grouping of maps according to spatial patterns

A visual comparison of the different maps for SLA, N and P indicated striking differences between the maps for each trait but no obvious grouping or similarities at first sight (Fig. S6). However, we found that the maps of SLA and N both clustered according to the use of PFT information for the upscaling of in-situ trait information: approaches using this additional information ('PFT + Env') were similar among each other and different from the other approaches that mostly used only environmental predictors ('Env') (Fig. 3a). The first two axes of the PCA explained 65% and 56% of the variance for SLA and N, respectively. The patterns in the PCA biplots were confirmed by pairwise correlation analyses showing a higher degree of within-group correlations for the approaches that used PFT information (Fig. 3b). The local correlations were moderately strong for the PFT + Env category but were zero for the Env category. High local correlations between maps from the PFT + Env group coincided with grid cells of high within-cell trait heterogeneity (Fig. S7b). For N, the PCA results were generally similar as for SLA (Fig. 3a) although one of the two Env maps did not fall into either group and showed low correlations to all other maps. The first two axes of the PCA explained 50%–60% of the variance. For P, only maps based on the use of PFT and environmental information were available. They showed similar global pairwise correlations as for SLA, but higher values for the homogeneous grid cells and slightly lower local correlation when all or the heterogeneous grid cells were selected (Fig. 3b).

3.1.2. Spatial patterns: between and within-group differences

We grouped the maps according to their use of PFT information and calculated the trait averages over all maps within a given category as well as the coefficient of variation (CV) for each grid cell as a metric for dissimilarity (Fig. 4). These 'synthesis maps'and corresponding CV maps of SLA and N differed strongly between the PFT + Env and Env groups (Fig. 4). On average, the CV values within the PFT + Env group were lower than in the Env group. Despite the higher level of similarity of the PFT + Env maps compared to the Env maps (Figs. 3b, 4, S8), there were notable differences between individual PFT + Env maps of all three traits such as the much higher trait values of the Butler maps at high latitudes (Fig. S6, Fig. S8).

Across traits the average PFT + Env maps showed a close correspondence between spatial patterns of traits and land cover, whereas the average Env maps did not (Fig. 4, 5a). For SLA, the PFT + Env mean map had high values in regions dominated by GRA, and SHR PFTs and a distinct band of low values for ENF (Figs. 4, 5a). The Env mean map, in contrast, showed - overall low values in the Southern Hemisphere and a band of higher values in parts of the Northern Hemisphere dominated by GRA and ENF (Figs. 4, 5a). For N, the PFT + Env mean map showed somewhat similar patterns with a band of low values in the ENF dominated areas, while the Env mean map had overall high values with little contrast between the Northern and Southern Hemispheres. Also when looking at Europe in more detail (Fig. 4), the PFT + Env maps for SLA and N showed spatial patterns corresponding to dominant LCTs while the Env maps showed little contrast between dominant LCTs. For P, the mean PFT + Env map showed the lowest values in EBF-dominated regions and clearly lower values in the Southern than the Northern Hemisphere. P had somewhat lower values in the ENF-dominated region compared to the surrounding areas but the contrast was smaller than for SLA and N.

3.2. Evaluation of upscaled global trait maps with sPlotOpen

While it is instructive to compare the trait distributions of upscaled maps to those of *plot*-level sPlotOpen data (Fig. S9, S10), the interpretation is somewhat complex (Discussion 4.4.2). Therefore, we focus on the comparison of upscaled maps to sPlotOpen data scaled to the grid cells in the following results description.

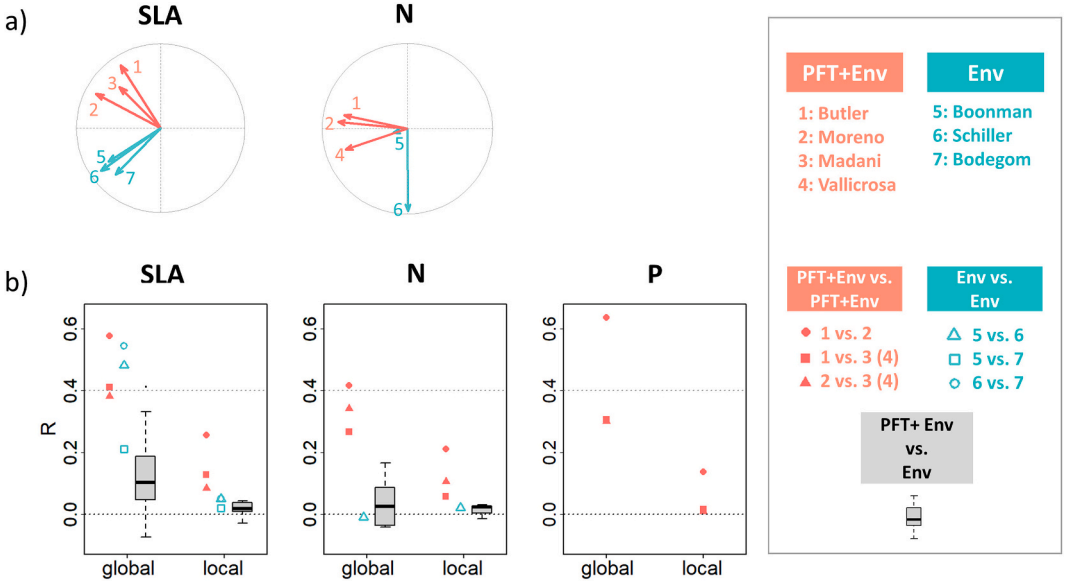

Fig. 3. Overview of principal component analyses and pairwise correlation of upscaled maps or specific leaf area (SLA), leaf nitrogen (N) and phosphorus (P) concentration. In the principal component biplots with the first two axes a) and the pairwise correlation plots b), colors correspond to the use of predictor variables ('Env' stands for environmental variables, while 'PFT' stands for plant functional type and land cover type information). Pearson correlation is shown either for all selected grid cells ('global') or as median value of the local spatial correlation map in 3 × 3 pixel windows ('local'). In b) the gray boxplots contain all possible pairs of PFT + Env maps and the Env maps; for the PFT + Env maps, the same symbols are used for the cases 'x vs. 3' and 'x vs. 4', as 3 is only available for SLA and 4 only for N and P; note that the symbols for P and the case '1 vs. 2' and '2 vs. 4' are so close that they are hard to distinguish visually.

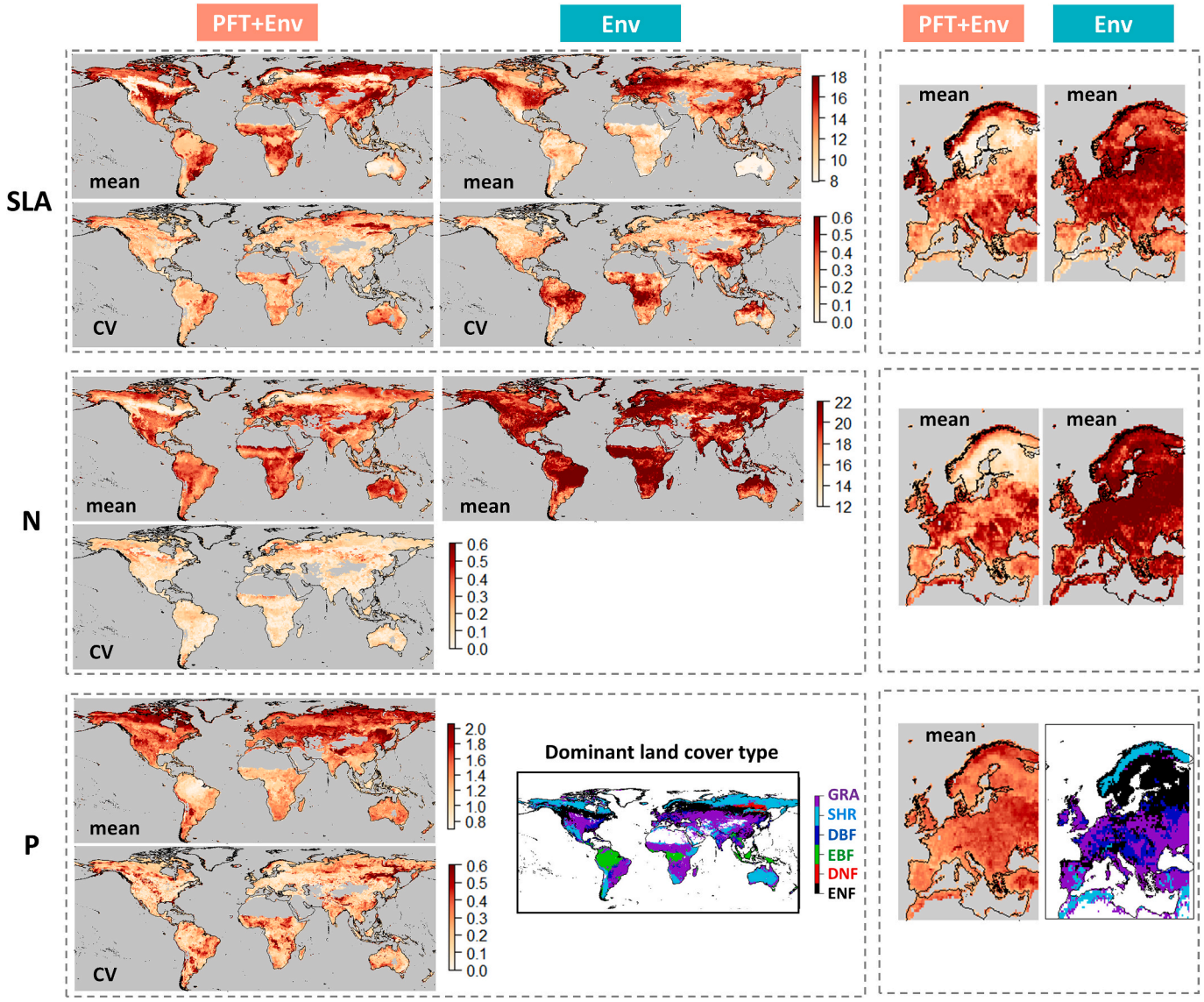

Fig. 4. Overview of spatial patterns of specific leaf area (SLA, mm^2/mg), leaf nitrogen (N, mg/g) and phosphorus (P, mg/g) for different upscaled maps. For each trait, the the upper row shows the average and the lower row shows the coefficient of variation (CV) between the maps of each upscaling category: those that used both plant functional type and environmental information (PFT + Env) and those that use mostly only environmental predictors (Env). The average trait maps for Europe are shown besides the global maps and have the same color scales as the corresponding global maps. The global and European maps of dominant land cover type are shown for reference (ENF: evergreen needleleaf forest; DNF: deciduous needleleaf forest; EBF: evergreen broadleaf forest; DBF: deciduous broadleaf forest; SHR: shrubland; GRA: grassland).

3.2.1. With PFT stratification

We found large differences between upscaled maps regarding both the spread of trait values between PFTs and the absolute values (Fig. 5b). A general tendency was that the PFT + Env maps showed larger spread between PFTs than the Env maps. This larger spread of the PFT + Env maps was more consistent with grid-level sPlotOpen data for SLA and N than for the Env maps even when considering the difference between TWM vs. CWM. While CWM showed smaller between-PFT differences than TWM, they were still clearly visible and had mostly similar patterns between PFTs (Fig. 5b). The description of results focuses on mean PFT trait values for the sake of simplicity, but the differences in spread between PFTs can also be observed across latitudinal gradients (Figs. S11, S12).

For SLA, only the Butler map had a similar level of spread between PFTs as sPlotOpen TWM and was the only map that came close to matching the low values for ENF (Fig. 5b). However, the Butler map had much higher values for SHR than sPlotOpen and EBF was also considerably higher but these discrepancies were due to specific latitudinal ranges and agreement in others was considerably better (Fig. S12). The other two PFT + Env maps (Moreno, Madani) were more consistent with sPlotOpen in terms of the order of PFTs, but had considerably smaller between-PFT differences (even smaller than for CWM). While the Env maps differed somewhat in the absolute values, they generally tended to have the highest values for ENF and the lowest values for SHR and GRA, which was opposed to the patterns in sPlotOpen CWM (Fig. 5b).

For N, the difference in values for ENF among the PFT + Env maps was smaller than for SLA, but the differences in spread between PFTs and the order of PFTs were still considerable (Fig. 5b). Similar to SLA, Butler showed higher values for SHR and EBF than sPlotOpen TWM and showed more similar values for DBF and GRA. As for SLA, Moreno showed a similar order of PFTs as sPlotOpen but even smaller spread than CWM. The Vallicrosa maps showed large differences between ENF and DBF but very similar values for the other PFTs. The two Env maps

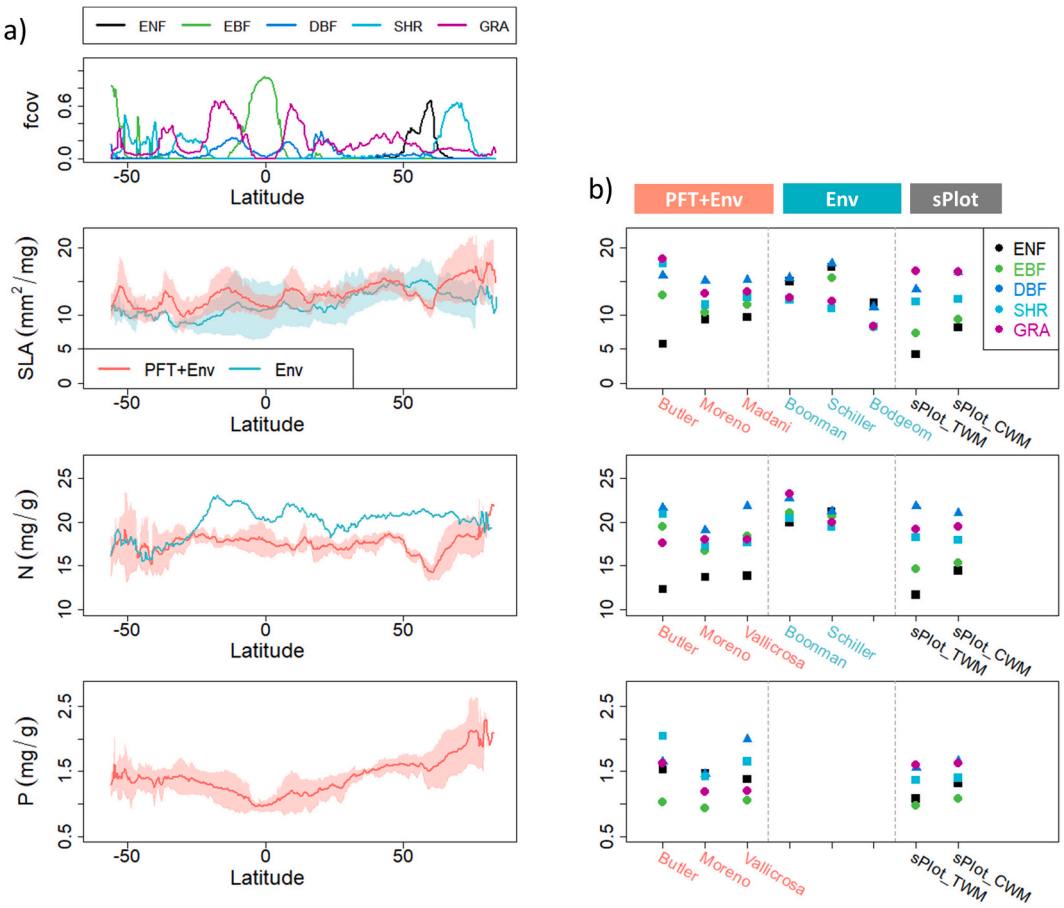

Fig. 5. Latitudinal patterns of upscaled trait maps and differences between plant functional types (PFTs). a) Median latitudinal trait values of fractional PFT cover (fcov) and median latitudinal trait values of specific leaf area (SLA), leaf nitrogen (N) and phosphorus contents (P) averaged over the two upscaling groups (PFT + Env vs. Env). The shading around the mean values indicates one standard deviation in cases where there were at least three maps. b) Comparison of mean PFT (fcov >0.5) trait values per upscaling approach with colors indicating each PFT (ENF: evergreen needleleaf forest; EBF: evergreen broadleaf forest; DBF: deciduous broadleaf forest; SHR: shrubland; GRA: grassland). TWM indicates top-of-canopy weighted mean, and CWM includes all vertical layers (see Table 1).

overall had much smaller spread between PFTs than the other upscaled maps and sPlotOpen.

For P, the Butler and Vallicrosa maps showed larger differences between PFTs than sPlotOpen, while the Moreno map had a more similar level of differences (Fig. 5b). There was little similarity in the absolute values between sPlotOpen and the upscaled maps except for EBF which consistently had the lowest values for the upscaled maps and sPlotOpen. The difference between TWM and CWM was considerably smaller for P than for SLA and N.

We found considerable differences between upscaled maps regarding their agreement with sPlotOpen in terms of the within-PFT trait variation. Moreover, different maps showed the best agreement with sPlotOpen for any given trait and PFT with none of the maps clearly showing the overall best performance (Fig. S12).

We found rather low grid-cell to grid-cell correlations of the upscaled maps vs. sPlotOpen at the level of individual PFTs/LCTs. Moderate to strong correlations only emerged when pooling data from all PFTs/LCTs (Fig. S13). In particular, the Butler maps showed high correlations with the difference to the Moreno map mostly being its lower SLA and N values for ENF. The improved Butler categorical maps showed a similar level of correlation as the PFT + Env map confirming that the correlation in the results with pooled data is strongly driven by between-PFT trait differences.

3.2.2. *Without PFT stratification*

Overall, we found that the upscaled maps showed moderate correlations (R up to 0.6) to sPlotOpen when matching the leaf-to-grid scaling strategy (unweighted average vs. average weighted by fractional land cover) of sPlotOpen to that of the upscaled maps (Fig. 6a for PFT + Env maps, Fig. 6b for Env maps). When comparing upscaled maps to sPlotOpen scaled to the grid cell with a different approach than was used in the upscaling approaches (Fig. 6b for PFT + Env maps, Fig. 6a for Env maps), the correlations to sPlotOpen were considerably lower for SLA and N (R = 0.2–0.4). For P, however, there were large differences between the scaling options for the PFT + Env maps but they did not follow the same pattern as for SLA and N except for the Butler Env map. In particular, the highest correlation of PFT + Env maps (Moreno) to sPlotOpen was to CWM without land cover weighting.

Even when only considering consistent leaf-to-grid scaling of sPlotOpen and the upscaled maps, there were notable differences between individual maps of the upscaling categories (Fig. 6). In the group of PFT + Env maps, the Butler map agreed best with sPlotOpen cover-weighted TWM and the (optimized) categorical map (PFT) showed similar performance as the full upscaled map. The Moreno map showed similar agreement to sPlotOpen cover-weighted TWM as Butler for SLA, but lower correlation for N and higher correlation for P (Fig. 6a). However, the Moreno map tended to agree better with sPlotOpen unweighted (at grid cell level) CWM, with considerable differences for SLA and P and similar correlation for N (Fig. 6b). Among the Env maps, the Schiller map showed consistently better agreement to sPlotOpen unweighted CWM data than the other maps, especially for N (Fig. 6b).

We found a tendency of stronger univariate trait-environment

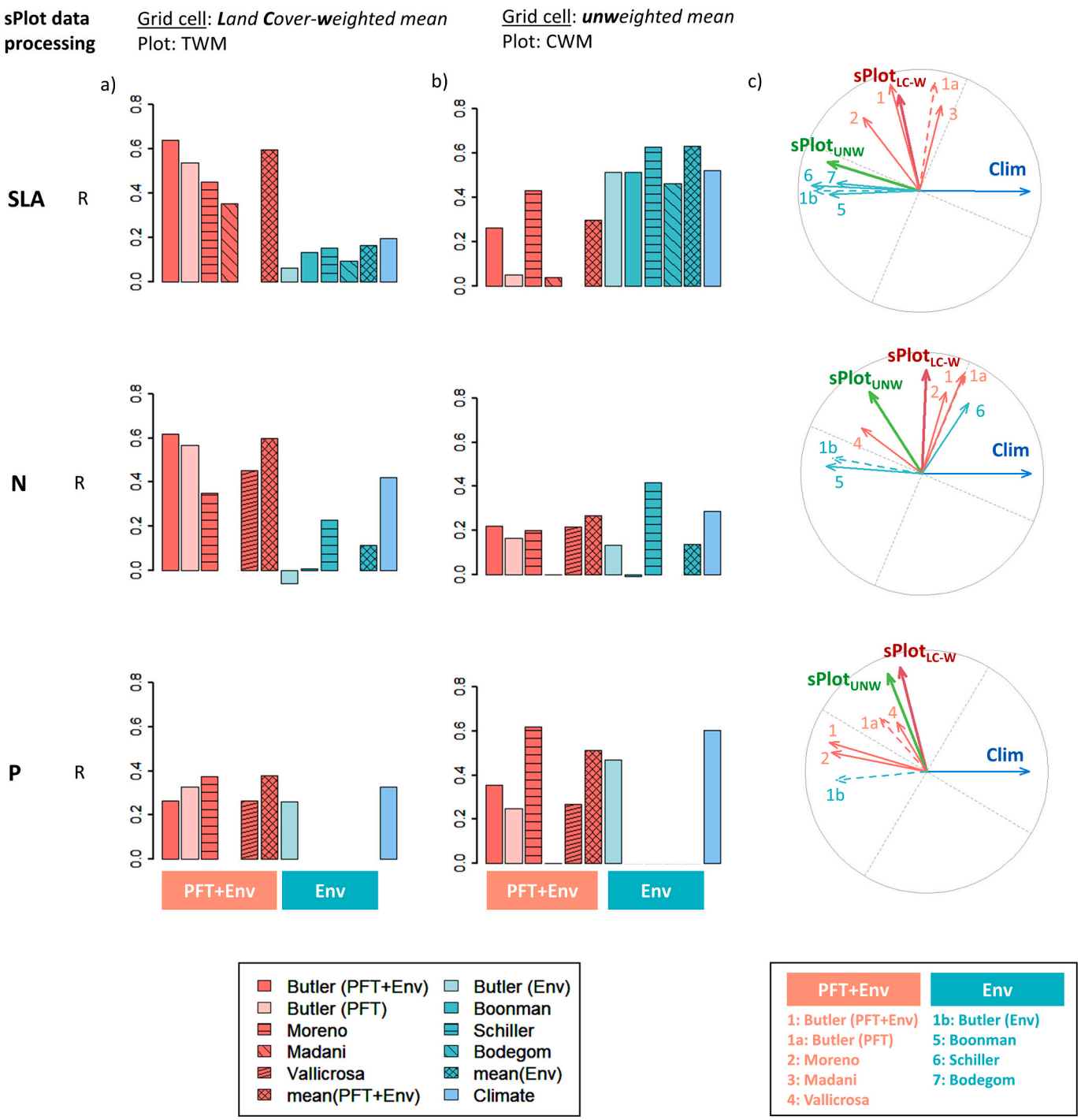

Fig. 6. Comparison of upscaled maps against grid-level sPlotOpen data at 0.5°. The left column a) shows the correlation between upscaled maps against top-of-canopy weighted mean (TWM) sPlotOpen data scaled to the grid by weighting with the land cover fraction (fcov) corresponding to each plant functional type of the. The middle column b) shows the correlation between upscaled maps and community weighted mean (CWM) sPlotOpen data scaled to the grid without weighting. Colors refer to the group of maps relying predominantly on environmental drivers (Env) or additionally also plant functional type and land cover information (PFT + Env). The blue colored bars indicate the highest correlation of sPlotOpen to a single environmental variable (among those used by Butler et al., 2017) per trait and sPlotOpen data processing case. The right column c) shows principal component biplots (first two axes) of upscaled maps, sPlotOpen data, and the climate variable (Clim) with the strongest relationships to Env maps (total annual solar radiation for SLA and N, mean annual temperature for P). In a) and b), the mean over the two upscaling groups excludes the different versions of Butler (only PFT, only Env) and the climate cases. (For interpretation of the references to color in this figure legend, the reader is referred to the web version of this article.)

relationships for the unweighted CWM grid cell mean sPlotOpen trait values compared to the land cover weighted TWM (Fig. 6b, c). This was most pronounced for SLA and P where a single environmental predictor showed similar levels of correlation to sPlotOpen data aggregated to grid cells without weighting as the 'best' upscaled Env maps.

4. Discussion

Overall, our findings indicate that users of upscaled foliar trait maps should carefully consider which approaches are suitable for their application given the fundamental differences between maps using PFT

and land cover information compared to those that did not (Figs. 3, S6). Even within those two categories, there are considerable differences and the average of the respective maps did not outperform individual maps in the evaluation (Fig. 6). This suggests, that comparing downstream results based on different individual maps is preferable to using the averages of maps from one of the two upscaling categories.

4.1. Upscaling with or without PFT and land cover information?

Both the PFT + Env and the Env upscaling approaches have practical advantages and limitations which partly depend on the characteristics of the in-situ data. We found that the Env-based maps do not capture the between-PFT trait differences (Fig. 5b) and tend to show stronger similarity to key environmental drivers (Figs. 6, 7c, Figs. S14, S15), while they apparently reasonably capture environmentally driven within-PFT variations (Fig. S12). This is directly opposed to the categorical maps that only rely on PFT information to represent between-PFT differences while, by design, lacking information on within-PFT trait variation (Fig. 7c, Table S5). PFT + Env approaches can combine the two to capture both between- and within-PFT trait variation (Figs. 5b, 7, S9, S12). The benefits of including PFT information depend on the level of between-PFT differences of the targeted trait, with SLA and N showing

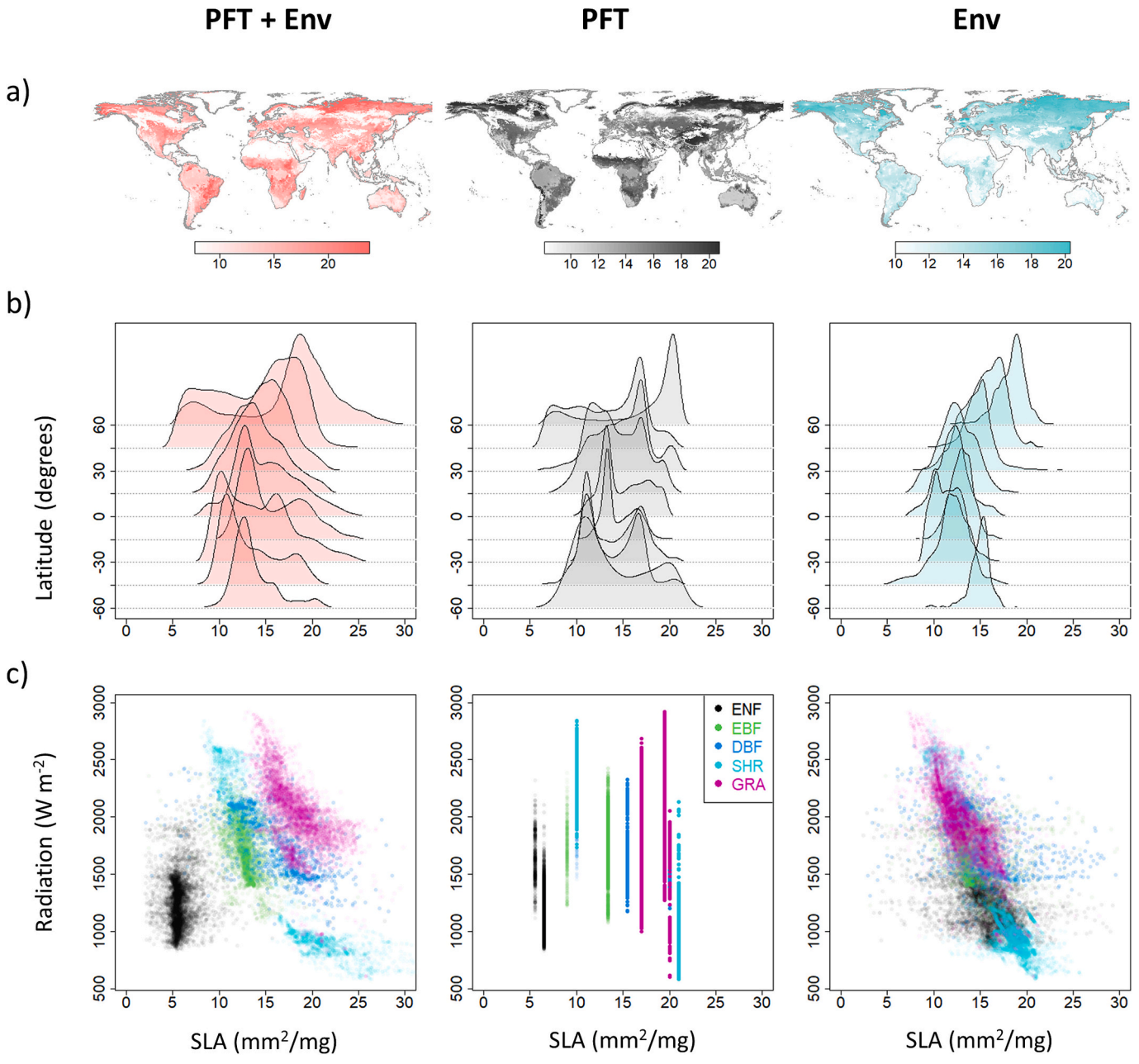

Fig. 7. Overview of the impact of different upscaling approaches on maps, latitudinal trait distributions and the corresponding trait-environment relationships using consistent trait inputs and processing. a) maps of specific leaf area (SLA) for three different upscaling approaches applied to the same in-situ top-of-canopy weighted mean (TWM) data by Butler et al. (2017): the full upscaling model ('PFT + Env') using environmental predictors, plant functional type (PFT) and land cover information, the simplified categorical map ('PFT') only relying on land cover fractions and mean PFT trait values for 14 PFT categories, and the maps only relying on environmental predictors ('Env'). The color scales are optimized to maximize contrast for each map. b) the latitudinal distributions corresponding to the maps. c) the relationships between annual mean daily total solar radiation and the SLA values of the maps shown in a) stratified by land cover type (ENF: evergreen needleleaf forest; EBF: evergreen broadleaf forest; DBF: deciduous broadleaf forest; SHR: shrubland; GRA: grassland). For each land cover type only grid cells with >50% cover are shown.

larger differences between PFTs than P (Fig. 5b). Our results show that although including PFT information appears necessary to capture between-PFT trait differences in the upscaling approaches we examined, it is not sufficient to guarantee good performance (Figs. 5a, S9, Table S5).

4.1.1. Motivation and limitations of upscaling using PFTs

Motivations for using PFT information in trait upscaling can be by the refinement of oversimplified representations in PFT-based land surface models or aspects more directly related to the upscaling itself. Regarding the latter, we identified four main aspects:

(1) *PFTs as tool to account for the lack of representativeness of in-situ observations (leaf-to-grid scaling)*. In-situ trait observations in trait databases such as TRY (Kattge et al., 2020, 2011) were not designed to be representative of large (1 km or 50 km) grid cells but to characterize plant species, which are grouped to PFTs. To account for this lack of geographic representativeness, two strategies can be applied. First, averaging traits per PFT within each grid cell and then weighting by PFT cover fraction using land cover products before applying the spatialization (Moreno). Such approaches have also been applied for scaling canopy structure-related in-situ trait observations to larger grid cells in heterogeneous landscapes (Hufkens et al., 2008; Shi et al., 2015). Second, separately upscaling per PFT before combining them in a final step using LCT data (Butler, Madani, Vallicrosa). The basis for both strategies is that the within-grid cell trait variability is considerably reduced when stratifying by PFT, reaching a reduction of about 50% for SLA TWMs (Fig. 8b) which is consistent across a wide range of spatial scales (Fig. S16). As this reduction corresponds to between-PFT trait differences (Fig. 5b), similar results are expected for N but a smaller reduction for P.

(2) *PFT as useful categorical predictor (spatialization)*. As trait-environment relationships can differ between PFTs (Fyllas et al., 2020; e.g. Wright et al., 2005), including PFT information can considerably improve their predictive performance (Kambach et al., 2023; e.g. Reich et al., 2007).

(3) *Land cover as additional spatial constraint (spatialization)*. In addition to more robust within-PFT trait models, separately upscaling per PFT (Butler, Madani, Vallicrosa) effectively results in an additional spatial constraint on possible trait values in regions with sparse or no in-situ observations but reliable land cover information as the trait variation within a PFT tends to be smaller than across all PFTs. This can help reduce uncertainties in areas where environmental-based trait models tend to extrapolate.

(4) *Fractional land cover as tool to better represent traits in homogeneous grid cells (spatialization)*. Grid cells for which in-situ trait data are available are disproportionally heterogeneous in terms of land cover (Fig. 8a) (and hence also traits). This leads to narrower and more unimodal trait distributions in the grid cell- level training data than the plot-level in-situ data (Fig. S17a) and tends to propagate in upscaling approaches that do not explicitly use land cover weighting in the spatialization, i.e. Env approaches and the Moreno approach. However, the PFT + Env approaches with separate upscaling per PFT such as Butler are not affected by this as they effectively model homogeneous grid cells regarding land cover. Thus, they can "recover" the latitudinal trait distributions from in-situ data by better characterization of homogeneous grid cells in the spatialization step of the upscaling (Figs. 7b, S9).

Limitations of using PFT and land cover information. The PFT categories we used are based on the categorical traits growth form, leaf type and leaf phenology. They are useful in practice as they show clear differences in foliar traits (Fig. 5b, S11, also (Kattge et al., 2011)), can be reasonably well mapped from remote sensing, and – following the global spectrum of plant form and function (Díaz et al., 2016) - represent an optimal decomposition of trait distributions at this level. However, for some PFTs such as shrubs and grasslands, trait distributions are wide and show considerable overlap, which is not ideal. To better decompose trait variation, finer PFT categories could be used by e.g. separating shrubs into similar types as forest, distinguishing C3 and C4 grass and/or including additional phylogenetic characteristics (Anderegg et al., 2022). For upscaling there is a trade-off, however, as such finer PFT categories are harder to robustly capture at the global scale using currently available remote sensing information.

By definition, the LCT categories of the remote sensing-based LCT maps used in the upscaling only have a minimum cover threshold (Loveland and Belward, 1997) and therefore do not quantify the *actual* canopy cover which would be needed although progress in this direction is being made (Discussion 4.5). Also, the land cover maps can have considerable uncertainties even when considering only the original land cover class definitions (Congalton et al., 2014). Given these uncertainties and dominant impacts of the land cover information at both the global and local scales (e.g. Figs. 3b, Fig. S18), the differences between the PFT + Env maps could therefore be partly explained by discrepancies between the land cover products used by the different

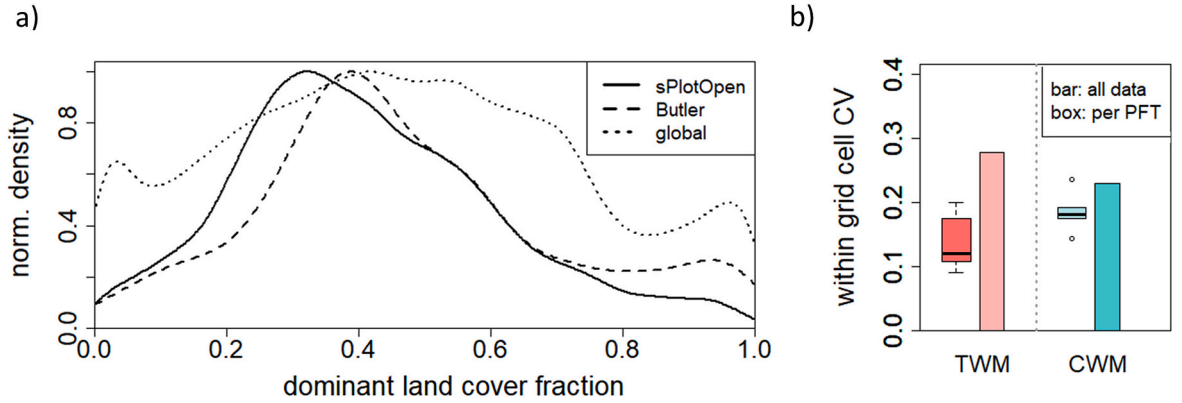

Fig. 8. Land cover heterogeneity at the grid-cell level and reduction of its impacts on trait heterogeneity by using plant functional type (PFTs). a) distribution of 0.5° grid cells regarding the maximum land cover fraction irrespective of the land cover type: sPlotOpen (all plots, N ~ 5000), TRY data selected by Butler et al. (2017)(N ~ 500), or all global vegetated grid cells (N ~ 60,000). The maximum fraction represents a measure of land cover homogeneity. b) sPlotOpen global-scale within grid cell (0.5°) trait variability as quantified by the coefficient of variation (CV) based on top-of-canopy weighted mean (TWM) or community weighted mean (CWM) data and all available trait data (bar showing median over the global-scale distribution) or stratified per PFT (boxplot summarizing the global medians of the individual plant functional types, i.e., PFTs).

upscaling approaches (Table S2).

4.1.2. Motivation and limitations of upscaling without PFTs

Due to the limitations of PFT categories and LCT products, upscaling without them can seem preferable conceptually. Upscaling approaches without using PFT information could be used for estimating future changes in foliar traits (e.g. Boonman et al., 2022) without the need for future land cover predictions which likely have higher uncertainties than the corresponding climate predictions from Earth System Models. Upscaling approaches that do not rely on PFT information, however, face important practical limitations.

Limitations in leaf-to-grid scaling. In the leaf-to-grid scaling, the unweighted averaging over available in-situ data effectively assumes either that these data are representative of the grid cells or that there might be biases at smaller scales that average out when looking at global scale trait patterns. The assumption of representativeness is not well justified as laid out in 4.1.1 (aspect 1) above. Simply increasing the number of observations without a dedicated sampling design does not decrease the level of land cover heterogeneity (Fig. 8a). This reasoning also applies to

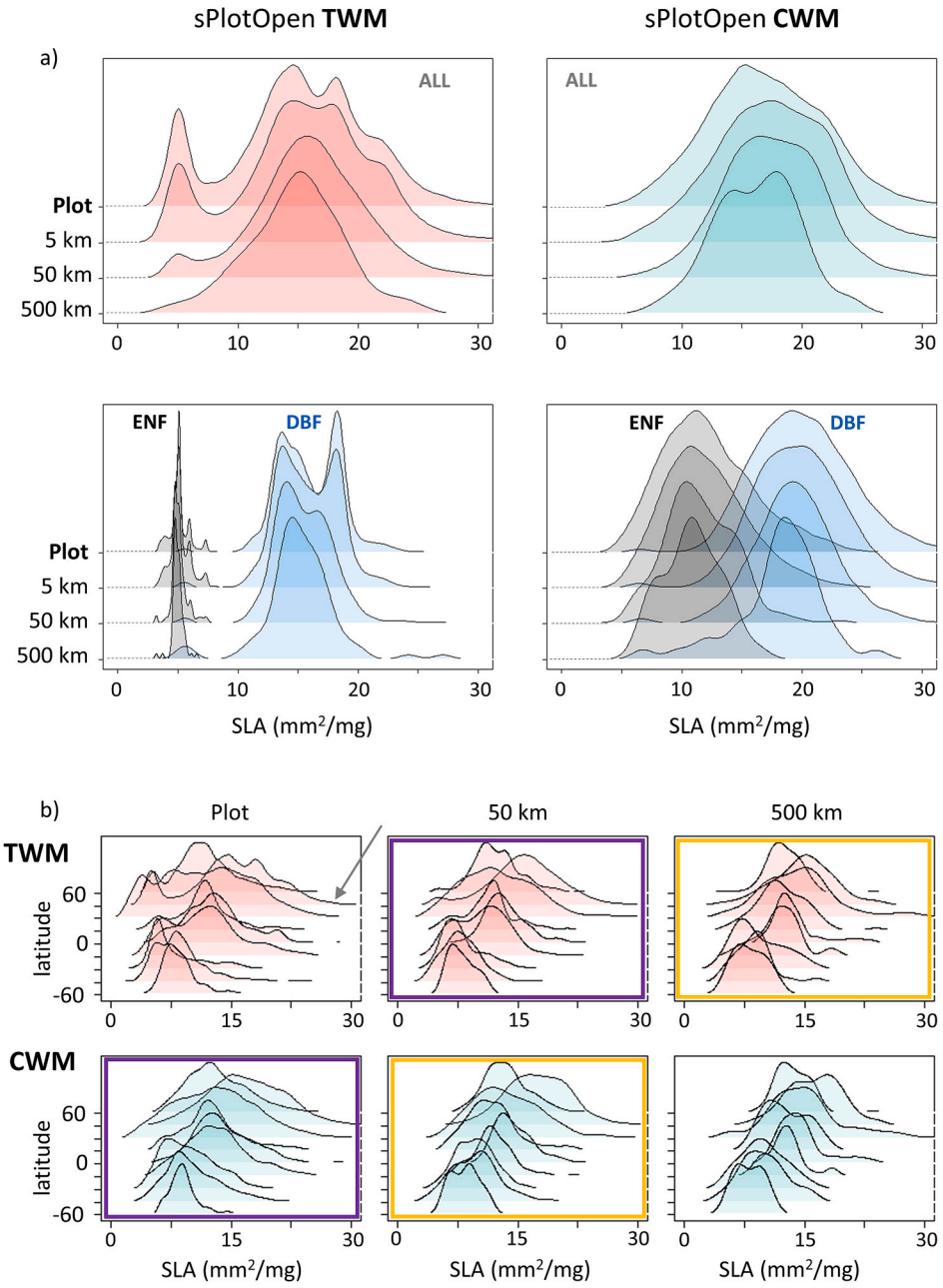

Fig. 9. Impacts of unweighted scaling to grid cells on latitudinal trait distributions across a range of spatial resolutions. a) example of the impacts of unweighted averaging on sPlotOpen top-of-canopy weighted mean (TWM) and community weighted mean (CWM) trait distributions in the latitudinal range of 45°-60° north either including all data ('All' in top row) or stratified by PFT for evergreen needleleaf forest (ENF) and deciduous broadleaf forest (DBF). Plot data are shown for reference and three different grid cell sizes with their corresponding size at the equator are given. b) global latitudinal trait distributions for sPlotOpen TWM (top row) and CWM (bottom row). The gray arrow in the top-left panel indicates the distribution corresponding to the latitudinal range in a). The colored purple and orange boxes highlight similar distribution patterns between TWM and CWM cases. (For interpretation of the references to color in this figure legend, the reader is referred to the web version of this article.)

upscaling approaches that first spatialized and then scaled a much higher number of trait estimates to the grid cell (Schiller and Wolf et al., 2022) as the additional data is not based on sampling grid cells with homogeneous land cover. Increasing the spatial resolution of grid cells also does not necessarily result in lower land cover heterogeneity which is high even for the 1 km grid cells used by Moreno and Vallicrosa (Yu et al., 2018).

The impacts of the lack of representativeness of in-situ observations on upscaled maps are not limited to small spatial scales such as neighborhoods of a few 0.5° grid cells but are visible at the global scale. This is most conspicuous in the boreal forest region dominated by ENF (Figs. 4, 5) where unweighted leaf(or plot)-to-grid scaling averages out the large differences in SLA and N between ENF (low trait values) and other LCTs such as DBF and SHR (high trait values) (Figs. 9a, S19). This effect of suppression of the low trait values for ENF in upscaled maps without PFT information (Bodegom, Boonman, Schiller) can also be seen in the Env versions of the Butler and Moreno upscaled maps (Figs. S14x, S19x) demonstrating that this effect is indeed caused by the unweighted averaging within grid cells and not by other factors. Importantly, the impacts of unweighted scaling from leaf (or plot) level to grid cells show a strong dependence on grid cell size (Figs. 9a, S19xb). Although land cover-weighted aggregation to grid cells shows similar impacts on trait distributions as unweighted aggregation at first sight (Fig. S17a), the weighted aggregation is largely independent of grid cell size as sub-grid information is accounted for by the fractional land cover maps. This is supported by the finding that the Butler and Moreno maps showed the highest levels of correlations between upscaled maps (Fig. 3b) despite their large difference in original grid cell size (50 km for Butler vs. 1 km for Moreno).

Limitations in the spatialization. Only using environmental information in the spatialization implies using universal trait-environment relationships across all vegetation types (Figs. 7c, S16), which results in limitations to capture trait differences between PFTs (Kambach et al., 2023; e.g. Reich et al., 2007). In principle, this limitation could be overcome by using additional predictors that contain information on PFTs/LCTs such as the satellite-based reflectance time series used by Moreno. However, we found that adding such predictors in the spatialization step still results in unrealistically small between-LCT differences unless between-PFT differences are also accounted for in the leaf-to-grid scaling, (Figs. S14a, S18a,b).

Another relevant aspect is that only using environmental predictors results in patterns that better represent *potential* vegetation that could grow in a certain place given the environmental conditions rather than the vegetation that is *actually* growing there (Table S5). Thus, a version of the Moreno maps that used PFT in the leaf-to-grid scaling but not the spatialization captured the between-PFT trait differences better but does not well reflect the actual land cover (Figs. S14, 18). Using remote sensing predictors in the spatialization as done by Moreno can overcome such limitations as direct information on surface characteristics is included (Table S5, Fig. S18), which is consistent with an analogous situation for species distribution modeling (Bonannella et al., 2022).

4.2. Vertical variation of traits within the canopy: upscaling CWMs or TWMs?

4.2.1. Conceptual role of CWM/TWM and impacts on spatial trait variations

Apart from the horizontal scaling aspects related to the use of PFTs and land cover, the differences in the upscaling approaches regarding the way vertical trait variation was accounted for is an important aspect to consider. Conceptually, CWM and TWM correspond to an intermediate step in the leaf-to-grid scaling and either combine all vegetation layers (CWM) or only the top-of-canopy layer (TWM) of a plant community. (Note that this may not account for different light environments as underlying trait data are typically based on sunlit leaves.) In the case of plot data such as sPlotOpen, CWM and TWM are approaches to scale leaf-level trait observations to the plot level before scaling plot-level traits to the grid cell level. While this separation of leaf-to-grid scaling into two steps is straightforward for sPlotOpen, it is more challenging to apply with TRY data, which is generally based on individual plants rather than vegetation plots. Boonman is the only upscaling approach that explicitly applied a (local) community mean (unweighted) on data from TRY by selecting datasets that well represent local plant communities before scaling to the grid cell. The PFT + Env approaches applied an unweighted mean per PFT, which resembles TWMs conceptually. The Env approaches Bodegom and Schiller and the Env versions of Butler and Moreno more closely resemble CWMs as all trait data in grid cells is averaged no matter to what vegetation layer it corresponds to. Therefore, in contrast to sPlotOpen data, it is challenging to apply an Env + PFT upscaling approach based on CWM when using TRY data. With the exception of Boonman, the correspondence of TRY-based upscaling approaches to sPlotOpen TWM and CWM seems to be a consequence of using PFT information or not rather than a conscious choice for one or the other trait metric.

Given the challenges of quantifying the impacts of CWM vs. TWM based on the existing upscaled maps, we used the sPlotOpen data for this purpose in an approach that corresponds to the first step of the upscaling (Fig. 1). We found that the use of CWMs versus TWMs has notably smaller impacts on spatial trait patterns than the scaling to the grid cells with PFTs and LCTs or unweighted aggregation, especially for N and P (Figs. S17xb). However, the impacts of CWM on plot-level latitudinal trait distributions are considerable for SLA (Fig. 9a) and closely resemble those of unweighted aggregation of TWM to 50 km grid cells (Fig. 9b), i.e. CWMs have narrower and more unimodal trait distributions with smaller differences between PFTs than TWM (Figs. 4b, 9, S9). The latitudinal patterns of CWM aggregated to 50 km resemble those of TWM at 500 km (Fig. 9b) with a less complex latitudinal pattern of overall increasing SLA with latitude. These findings indicate that the impacts of combining vertical vegetation layers in CWMs are similar to those of unweighted aggregation to large grid cells, as traits from different PFTs are combined in both cases.

4.2.2. Motivations for using CWM or TWM

CWMs are the standard metric for many ecological analyses based on community trait data (Anderegg, 2023; Bruelheide et al., 2018; Guerin et al., 2022) but there are large differences depending on the weighting factor used. In practice, the weighting of traits is commonly done by the basal area, biomass, or leaf area (Anderegg, 2023). For sPlotOpen, however, fractional species cover or abundance is used (Sabatini et al., 2021) as weighting factors more closely related to total leaf area are not available. The resulting CWM values based on such weighting not infrequently give comparable weight to overstory trees and understory in forest plots, despite the large differences in biomass. Therefore, for forests top-of-canopy-weighted means (TWMs), which neglect understory contributions, can be considered a pragmatic approximation of (leaf) biomass-weighted CWMs.

Apart from an approximation of biomass-weighted CWMs, upscaling TWMs can also have other motivations. First, from the perspective of terrestrial biosphere modeling, the higher levels of a canopy tend to dominate processes of vegetation-atmosphere interactions due to the dominance of leaf area and light availability of top-of-canopy vegetation (Musavi et al., 2015). Second, TWMs are a useful metric when aiming to link upscaled maps to maps more directly based on remote sensing approaches that tend to focus on the top of the canopy. Thus, upscaled plant height maps based on TWM show a considerably higher level of similarity to satellite-based canopy height maps using lidar information (Lang et al., 2022; Potapov et al., 2021; Simard et al., 2011; Wang et al., 2016) than CWM upscaled maps (Fig. S20). Importantly, the TWM and CWM upscaled maps differ not only considerably regarding their absolute values as expected but also show large differences in their spatial

patterns (Fig. S20). This is consistent with reports of impacts of different weighting approaches on the spatial patterns of upscaled foliar trait maps (Wang et al., 2016).

4.3. Other factors contributing to differences between upscaled maps

Although less important than using PFT and land cover information and the CWM vs. TWM distinction, other differences between upscaling approaches (Fig. 1) might be relevant. Thus, even when staying within one of the two upscaling categories (PFT + Env or Env), the differences in in-situ trait datasets and the selected predictor variables is expected to make a difference in the upscaled maps. Given the confounding factors, however, a dedicated sensitivity analysis would be needed to quantify these impacts, which goes beyond the scope of our study. Two studies (Boonman, Moreno) compared the impacts of using different regression algorithms in the spatialization step while keeping all other aspects of the upscaling stable. These studies found overall comparable performance of the different regression algorithms with twos exceptions (reported by Moreno) that were, however, not used by any of the other studies indicating overall small impacts of the choice of algorithm on the differences between the upscaled maps we compared.

4.4. Evaluation of maps

4.4.1. Internal performance metrics

Overall, there was a clear pattern of considerably higher cross-validation performance for PFT + Env approaches compared to Env approaches (R2 about 0.6 or higher for PFT + Env compared to 0.4 or lower for Env), with larger differences for N compared to SLA. However, these findings should be interpreted carefully given the limitations of random cross-validation approaches to evaluate mapping performance (Meyer and Pebesma, 2021; Ploton et al., 2020) as well as the dominant impacts of land cover on the PFT + Env maps. Some of the upscaling products also provided estimates of the uncertainty of the mean (standard error) trait values per grid cell but this was based on different methodology and should be interpreted with caution. Overall, we found no indications that the uncertainty or variability estimates corresponded to the observed discrepancies between maps, even within the PFT + Env and the Env groups (Figs. 4, S21x).

4.4.2. External reference data (sPlotOpen)

As the upscaling approaches differ in the way horizontal (within-grid-cell) and vertical (within canopy) trait variation was taken into account, there is no way to process sPlotOpen data such that it could be used as the universal benchmark for all upscaling approaches. Rather, sPlotOpen can be used as a basis for evaluating the differences in performance *within* a given upscaling framework/strategy regarding the leaf-to-grid scaling (unweighted aggregation vs. land cover fraction weighting) and the site or plot level trait metric, i.e. CWM or TWM.

Regarding the evaluation of PFT + Env maps with grid-cell-level sPlotOpen data, our results indicate that a comparison stratified per PFT (Figs. 5b, S11- S1) is more meaningful than at the level of the final maps. First, when using the final maps after applying the land cover-weighted averages, highly simplified categorical trait maps, which were the motivation for improvement using PFT + Env upscaling, can achieve a similar level of agreement with sPlotOpen reference data (Fig. 6a). To facilitate such evaluations at the level of individual PFTs, future upscaling products should be provided both as final global trait maps and its underlying PFT component maps. While we showed that the final maps can, in principle, be separated into PFT components (Text S2, Fig. S4), this approach introduces unnecessary additional uncertainties which can be avoided by using the direct outputs from the upscaling.

Comparing sPlotOpen *plot-level* data to upscaled maps can be useful to gain insights independent from the scaling from plots to grid cells but some aspects of the interpretation are challenging. Using *plot-level* sPlotOpen data can make better use of the considerably larger amount of plots compared to the number of grid cells that are covered and avoids the need to apply scaling to the grid cell, i.e. it allows only distinguishing between CWM and TWM. Meaningful comparisons between upscaled maps and sPlotOpen plot-level data can still be conducted by quantifying characteristics of the respective trait distributions such as latitudinal patterns (Figs. S9, S10). Despite the presence of mixed grid cells in the upscaled maps, the trait distributions prominently contain the signal of homogeneous grid cells (Figs. 7b, S9) such that a trait or land cover heterogeneity filtering of the maps is not necessary. While the interpretation of plot-level TWM sPlotOpen data to PFT + Env upscaled maps is rather straightforward, it is more complex for Env maps. The reason is that the plot-level CWM data show rather similar latitudinal trait distributions as those of TWM aggregated to 0.5° grid cells without weighting (Fig. 9b).

While sPlotOpen takes into account the species composition, it does not account for intra-specific trait variation. This might be a reasonable approach for large parts of the global vegetated land surface, but there could still be notable impacts in (dominant) species with wide geographic distributions. The large discrepancies between the high SLA and *P* values in the Butler maps and sPlotOpen seem to be partly caused by the large intraspecific variation in the in-situ data used in the Butler maps (Fig. S22), which raises the question to what degree including intraspecific trait variation would affect sPlotOpen-based trait estimates.

4.5. Future opportunities for foliar trait mapping using remote sensing data

Future upscaling efforts will benefit from advances in both the leaf-to-grid and spatialization steps (Fig. 1) with important contributions from remote sensing.

Advances have been ongoing to improve different aspects of remotely-sensed land cover. First, there is now a global, long-term product of 30 m land cover with a fine LCT classification system that includes the different forest types we have used (Zhang et al., 2024). This product can be used to generate fractional land cover at intermediate resolutions in an approach similar to that used by Moreno-Martínez et al. (2018) but without the need to downscale the much coarser MODIS 500 m or 1 km products. Second, given the increase in the availability of satellite imagery with both high spatial and temporal resolution (e.g. Houborg and McCabe, 2018), there is potential for and progress in improving land cover maps to better approximate actual PFT cover fractions (Harper et al., 2023; Macander et al., 2022; Wang et al., 2022a). Harper et al. (2023) used high-resolution (30 m) tree cover and canopy height maps to refine global, long-term land cover products in an attempt to better approximate actual PFT canopy cover. Wang et al. (2022b) applied a somewhat similar approach using only tree cover to Canada and Alaska. Macander et al. (2022) generated long-term, high resolution (30 m) top cover for seven PFTs across Alaska and parts of Canada. Also, individual tree crowns can now be detected at large scales (e.g. Mugabowindekwe et al., 2022; Wang et al., 2023) and could be further classified into PFTs e.g. in approaches similar to Harper et al. (2023). All these efforts could help reduce uncertainties in upscaled maps that use PFT information which also include approaches based on eco-evolutionary optimality theory (Dong et al., 2023) and process-based modeling (Goll et al., 2017; Thum et al., 2019; Zaehle and Friend, 2010).

Apart from improvements in land cover products, there are remote sensing-based approaches that more directly address uncertainties from the leaf-to-grid and spatialization steps using multi- and hyperspectral reflectance imagery.

To reduce uncertainties related to the leaf-to-grid scaling step, increasingly available high-resolution multispectral spaceborne imagery can be used to directly link it to in-situ ground reference data. For plot-level ground data, this can be done either in a single step using

sufficiently high-resolution imagery (Wan et al., 2024) or in two steps using multi-scale approaches based on satellite products with a trade-off in spatio-temporal resolutions (Xu et al., 2022). Even for ground measurements on individual tree canopies, multispectral satellite imagery and environmental predictors can be used to generate large-scale trait maps (Aguirre-Gutiérrez et al., 2021). Aguirre-Gutierrez et al. have already used this approach to generate foliar trait maps for the entire area covered by tropical evergreen broadleaf forests (under review). Potentially, such approaches could be extended to other forest ecosystems, potentially even without the need to incorporate explicit land cover maps given that imagery time series are used (Liu et al., 2024).

While multispectral satellite imagery has advantages in terms of spatio-temporal resolution and can be used to estimate foliar traits with strong absorption features such as chlorophyll content (Croft et al., 2020; Wan et al., 2024; Xu et al., 2022), hyperspectral reflectance data include information that is more directly linked to foliar traits such as SLA, N, pigment contents and phenolics (Féret et al., 2017; Jacquemoud et al., 1996; Kokaly, 2001; Kokaly and Skidmore, 2015). As the links between hyperspectral imagery and foliar trait is based on physical signals related to light absorption of foliar chemical components, the relatively weak environmental predictors might become unnecessary at least for estimating certain traits such as SLA and N. Also, alternatives to data-driven upscaling methods such as inversion of radiative transfer models can be applied to hyperspectral data to estimate key foliar traits (Tagliabue et al., 2019; Verrelst et al., 2015; Wan et al., 2024).

Hyperspectral-based trait estimation approaches can be used in different ways depending on the data availability. While the 30 m hyperspectral imagery available from the operational (PRISMA, EnMAP) and future (SBG and CHIME) missions cannot be directly linked to individual tree crowns, it can be directly linked to dedicated vegetation plots. Therefore, a global-scale network of sufficiently large vegetation plots needs to be established with intensive foliar trait sampling, also including the temporal dimension to capture sub-seasonal and interannual trait variations that impacts hyperspectral reflectance (Chlus and Townsend, 2022). While these efforts are ongoing, airborne high-resolution hyperspectral imaging can be used in a multi-scale, hybrid approach. This involves first bridging the scales between in-situ measurements on individual tree crowns or smaller plots and coarser grid cells to upscale to larger areas using multispectral satellite imagery and/or environmental predictors. Such approaches have been applied to generate foliar trait maps for Peru (Asner et al., 2016) and parts of the US (Liu et al., 2024) with maps for the entire CONUS currently in preparation (Liu et al., in prep.). Interestingly, the approach by Liu et al. (2024) neither requires environmental predictors nor LCT maps.

4.6. *Implications for the interpretation of remotely sensed plant trait maps*

While the focus of this study was on the comparison of upscaled foliar trait maps, our findings have important implications for the interpretation of currently available e.g. (Croft et al., 2020; Xu et al., 2022) and future plant trait maps more directly derived from remote sensing data (see 4.5 above). The challenge in the interpretation of such maps is that the dominant impact of land cover on plant trait maps can mask underlying ecological aspects of interest, e.g. regarding analyses of trait-environment relationships or climate change impacts. Therefore, combining remotely sensed plant trait maps with robust fractional land cover products is crucial.

The importance of land cover for the ecological interpretation of remotely sensed foliar trait maps may be relatively obvious but our study highlights an important aspect regarding details of their use that appears less widely recognized. First, due to the high levels of land cover heterogeneity even at higher spatial resolutions (1 km) (Yu et al., 2018), *fractional* land cover maps are needed. Second, to well extract trait variations within LCTs without "contamination" from land cover effects, setting high thresholds on land cover fractions is generally not sufficient as co-occurring LCTs can have strongly different trait values such as ENF and DBF for SLA and N (Figs. 2, S2). This makes it more challenging to conduct large-scale analyses of within LCT trait variations as "pure" grid cells covered by a single one of these LCTs only account for low fractions (at 1 km, the pure grid cell fractions of DNF, ENF and DBF are only about 15% according to Yu et al. (2018)). Combining thresholds on land cover fractions with thresholds on estimated trait variability as we did in case of the upscaled maps (Methods 2.4.2) does not lead to much higher fractions of retained grid cells at 0.5° resolution (Fig. S2), especially for ENF and DNF, so unmixing approaches as we applied might have to be used despite their limitations. When considering that many boreal forest ecosystems may not have a fully closed tree canopy, impacts of understory vegetation with very different trait values on remote sensing-based maps could be relevant despite apparently 100% coverage of e.g. ENF based on current land cover products that do not quantify canopy cover fractions. Therefore, airborne imaging spectroscopy campaigns such as NASA BOREAS (Sellers et al., 1997) and ABoVE (Miller et al., 2019) will remain an important tool to help interpret satellite-based foliar trait maps that do not have high enough resolution to resolve individual tree canopies.

5. Conclusions and recommendations

Despite differences in many aspects of the upscaling methodology, the use of PFT and land cover information was the dominant factor explaining the differences between the resulting maps, effectively dividing them into two different map categories with strongly differing spatial patterns. Differences in accounting for vertical trait variation (top-of-canopy versus community mean) were also relevant but had smaller impacts on the spatial patterns of foliar traits than the use of PFT and land cover data. Maps that used PFT and land cover information showed larger trait differences between PFTs and agreed better with sPlotOpen data than the maps mostly relying only on environmental predictor information. Not accounting for within-grid-cell trait variation tends to suppress extremes of the trait distributions, which effectively reduces trait differences between PFTs and leads to more unimodal trait distributions with larger impacts on top-of-canopy trait values. Importantly, these effects also show a strong dependence on grid cell size with greater impacts at larger grid cell sizes. While the use of PFT and land cover information can partly counteract these effects, the land cover information introduces other uncertainties and has dominant impacts on the global spatial patterns of trait variation. Our findings also have important implications for the ecological interpretation of foliar trait maps derived from more direct remote sensing approaches.

Based on the insights from our study, we identified five recommendations that are relevant for future efforts in generating and evaluating upscaled maps as well as interpreting foliar trait maps more directly based on remote sensing data:

1. Upscaling products should clearly specify the category of trait map provided, which is determined by the metric used at the site or plot level, the type of scaling to the grid cell level and the type of predictor information used. Upscaling products based on PFT information should provide the original maps for each PFT separately in addition to the overall product.
2. In the evaluation of maps with reference data such as sPlotOpen, comparable scaling as for the upscaled maps needs to be applied to the reference data if the grid cell size is much coarser than the plot size. Furthermore, comparisons of the distributions of *plot*-level reference data with those of upscaled maps can provide valuable additional insights. For maps using PFT and land cover information, an evaluation at the level of separately upscaled maps per PFT is recommended to directly quantify the agreement of between- and within-PFT trait variation independently of the impacts of land cover that dominate the final maps per trait.
3. Future upscaling efforts should aim at reducing the scale mismatch between in-situ observations and predictor data by increased efforts

to sample traits in sufficiently large plots and by using higher resolution predictor data, ideally with a stronger link to foliar traits than environmental variables such as hyperspectral imagery.
4. Future trait sampling efforts should consider the aspect of within grid cell trait variation due to land cover heterogeneity as well as representativeness at the global scale regarding geographic aspects and the relevant predictor information.
5. For ecological analyses of remote sensing-based foliar trait maps, quantifying trait variations within land cover types should be done by taking into account trait variability due to land cover, not only the heterogeneity of the land cover itself as the relationship between the two can be complex.

CRediT authorship contribution statement

Benjamin Dechant: Writing – review & editing, Writing – original draft, Visualization, Methodology, Investigation, Formal analysis, Data curation, Conceptualization. **Jens Kattge:** Writing – review & editing, Supervision, Funding acquisition, Data curation, Conceptualization. **Ryan Pavlick:** Writing – review & editing, Supervision, Funding acquisition, Conceptualization. **Fabian D. Schneider:** Writing – review & editing, Funding acquisition, Conceptualization. **Francesco M. Sabatini:** Writing – review & editing, Methodology, Data curation. **Álvaro Moreno-Martínez:** Writing – review & editing, Methodology, Data curation. **Ethan E. Butler:** Writing – review & editing, Data curation. **Peter M. van Bodegom:** Writing – review & editing, Data curation. **Helena Vallicrosa:** Writing – original draft, Data curation. **Teja Kattenborn:** Writing – review & editing, Data curation. **Coline C. F. Boonman:** Writing – review & editing, Data curation. **Nima Madani:** Writing – review & editing, Data curation. **Ian J. Wright:** Writing – review & editing. **Ning Dong:** Writing – review & editing. **Hannes Feilhauer:** Writing – review & editing. **Josep Peñuelas:** Writing – review & editing. **Jordi Sardans:** Writing – review & editing. **Jesús Aguirre-Gutiérrez:** Writing – review & editing. **Peter B. Reich:** Writing – review & editing. **Pedro J. Leitão:** Writing – review & editing. **Jeannine Cavender-Bares:** Writing – review & editing. **Isla H. Myers-Smith:** Writing – review & editing. **Holly Croft:** Writing – review & editing. **I. Colin Prentice:** Writing – review & editing. **Andreas Huth:** Writing – review & editing. **Karin Rebel:** Writing – review & editing. **Sönke Zaehle:** Writing – review & editing. **Irena Šímová:** Writing – review & editing. **Sandra Díaz:** Writing – review & editing. **Markus Reichstein:** Writing – review & editing, Conceptualization. **Christopher Schiller:** Writing – review & editing, Data curation. **Helge Bruelheide:** Writing – review & editing. **Miguel Mahecha:** Writing – review & editing. **Christian Wirth:** Writing – review & editing. **Yadvinder Malhi:** Writing – review & editing. **Philip A. Townsend:** Writing – review & editing, Supervision, Funding acquisition, Conceptualization.

Declaration of competing interest

The authors declare that they have no known competing financial interests or personal relationships that could have appeared to influence the work reported in this paper.

Data and code availability

Most underlying data of global foliar trait maps are already publicly available (see links given in Table S3). Other maps can be requested from the first authors (Table 1). The code for the calculation of sPlotOpen TWM data is available online (https://github.com/fmsabatini/sTraits_GlobalIntercomparison). Other code used relied on existing functions of R packages that are specified in the methods section.

Acknowledgements

This paper is a joint effort of the working group sTRAITS kindly supported by sDiv, the Synthesis Centre of the German Centre for Integrative Biodiversity Research (iDiv) Halle-Jena-Leipzig, funded by the German Research Foundation (DFG) (FZT 118, 02548816). Support for P.T., J.C.-B. and E.B. was provided by the NSF Biology Integration Institute ASCEND (DBI 2021898), with additional support for P.T. provided by NSF Macrosystems Biology and NEON-Enabled Science (MSB-NES) award DEB 1638720. A portion of this research was carried out at the Jet Propulsion Laboratory, California Institute of Technology, under a contract with the National Aeronautics and Space Administration (80NM0018D0004). This research was also supported by the European Research Council under the ERC-SyG-2019 USMILE project (grant agreement 855187). T.K. acknowledges funding from DFG for the project PANOPS (grant-no: 504978936). J.A.-G. was funded by the Natural Environment Research Council (NERC; NE/T011084/1) and the Oxford University John Fell Fund (10667). I.H.M.-S. was funded by the NERC grants ShrubTundra (NE/M016323/1) and Tundra Time (NE/W006448/1).

Appendix A. Supplementary data

Supplementary data to this article can be found online at https://doi.org/10.1016/j.rse.2024.114276.

References

Aguirre-Gutiérrez, J., Rifai, S., Shenkin, A., Oliveras, I., Bentley, L.P., Svátek, M., Girardin, C.A.J., Both, S., Riutta, T., Berenguer, E., Kissling, W.D., Bauman, D., Raab, N., Moore, S., Farfan-Rios, W., Figueiredo, A.E.S., Reis, S.M., Ndong, J.E., Ondo, F.E., N'ssi Bengone, N., Mihindou, V., Moraes de Seixas, M.M., Adu-Bredu, S., Abernethy, K., Asner, G.P., Barlow, J., Burslem, D.F.R.P., Coomes, D.A., Cernusak, L. A., Dargie, G.C., Enquist, B.J., Ewers, R.M., Ferreira, J., Jeffery, K.J., Joly, C.A., Lewis, S.L., Marimon-Junior, B.H., Martin, R.E., Morandi, P.S., Phillips, O.L., Quesada, C.A., Salinas, N., Schwantes Marimon, B., Silman, M., Teh, Y.A., White, L.J. T., Malhi, Y., 2021. Pantropical modelling of canopy functional traits using Sentinel-2 remote sensing data. Remote Sens. Environ. 252, 112122 https://doi.org/10.1016/j.rse.2020.112122.

Anderegg, L.D.L., 2023. Why can't we predict traits from the environment? New Phytol. https://doi.org/10.1111/nph.18586, 237, 1998-2004.

Anderegg, L.D.L., Griffith, D.M., Cavender-Bares, J., Riley, W.J., Berry, J.A., Dawson, T. E., Still, C.J., 2022. Representing plant diversity in land models: an evolutionary approach to make "functional types" more functional. Glob. Chang. Biol. 28, 2541–2554. https://doi.org/10.1111/gcb.16040.

Asner, G.P., Knapp, D.E., Anderson, C.B., Martin, R.E., Vaughn, N., 2016. Large-scale climatic and geophysical controls on the leaf economics spectrum. Proc. Natl. Acad. Sci. 113, 201604863. https://doi.org/10.1073/pnas.16048631.

Bonannella, C., Hengl, T., Heisig, J., Parente, L., Wright, M.N., Herold, M., de Bruin, S., 2022. Forest tree species distribution for Europe 2000–2020: mapping potential and realized distributions using spatiotemporal machine learning. PeerJ 10, e13728. https://doi.org/10.7717/peerj.13728.

Bongers, F.J., Schmid, B., Bruelheide, H., Bongers, F., Li, S., von Oheimb, G., Li, Y., Cheng, A., Ma, K., Liu, X., 2021. Functional diversity effects on productivity increase with age in a forest biodiversity experiment. Nat. Ecol. Evol. 5, 1594–1603.

Boonman, C.C.F., Benítez-López, A., Schipper, A.M., Thuiller, W., Anand, M., Cerabolini, B.E.L., Cornelissen, J.H.C., Gonzalez-Melo, A., Hattingh, W.N., Higuchi, P., Laughlin, D.C., Onipchenko, V.G., Peñuelas, J., Poorter, L., Soudzilovskaia, N.A., Huijbregts, M.A.J., Santini, L., 2020. Assessing the reliability of predicted plant trait distributions at the global scale. Glob. Ecol. Biogeogr. 29, 1034–1051. https://doi.org/10.1111/geb.13086.

Boonman, C.C., Huijbregts, M.A., Benítez-López, A., Schipper, A.M., Thuiller, W., Santini, L., 2022. Trait-based projections of climate change effects on global biome distributions. Divers. Distrib. 28, 25–37.

Bruelheide, H., Dengler, J., Purschke, O., Lenoir, J., Jiménez-Alfaro, B., Hennekens, S.M., Botta-Dukát, Z., Chytrý, M., Field, R., Jansen, F., Kattge, J., Pillar, V.D., Schrodt, F., Mahecha, M.D., Peet, R.K., Sandel, B., van Bodegom, P., Altman, J., Alvarez-Dávila, E., Arfin Khan, M.A.S., Attorre, F., Aubin, I., Baraloto, C., Barroso, J.G., Bauters, M., Bergmeier, E., Biurrun, I., Bjorkman, A.D., Blonder, B., Čarni, A., Cayuela, L., Černý, T., Cornelissen, J.H.C., Craven, D., Dainese, M., Derroire, G., De Sanctis, M., Díaz, S., Doležal, J., Farfan-Rios, W., Feldpausch, T.R., Fenton, N.J., Garnier, E., Guerin, G.R., Gutiérrez, A.G., Haider, S., Hattab, T., Henry, G., Hérault, B., Higuchi, P., Hölzel, N., Homeier, J., Jentsch, A., Jürgens, N., Kącki, Z., Karger, D.N., Kessler, M., Kleyer, M., Knollová, I., Korolyuk, A.Y., Kühn, I., Laughlin, D.C., Lens, F., Loos, J., Louault, F., Lyubenova, M.I., Malhi, Y., Marcenò, C., Mencuccini, M., Müller, J.V., Munzinger, J., Myers-Smith, I.H., Neill, D. A., Niinemets, Ü., Orwin, K.H., Ozinga, W.A., Penuelas, J., Pérez-Haase, A.,

Petřík, P., Phillips, O.L., Pärtel, M., Reich, P.B., Römermann, C., Rodrigues, A.V., Sabatini, F.M., Sardans, J., Schmidt, M., Seidler, G., Silva Espejo, J.E., Silveira, M., Smyth, A., Sporbert, M., Svenning, J.-C., Tang, Z., Thomas, R., Tsiripidis, I., Vassilev, K., Violle, C., Virtanen, R., Weiher, E., Welk, E., Wesche, K., Winter, M., Wirth, C., Jandt, U., 2018. Global trait–environment relationships of plant communities. Nat. Ecol. Evol. 2, 1906–1917. https://doi.org/10.1038/s41559-018-0699-8.

Bruelheide, H., Dengler, J., Jiménez-Alfaro, B., Purschke, O., Hennekens, S.M., Chytrý, M., Pillar, V.D., Jansen, F., Kattge, J., Sandel, B., Aubin, I., Biurrun, I., Field, R., Haider, S., Jandt, U., Lenoir, J., Peet, R.K., Peyre, G., Sabatini, F.M., Schmidt, M., Schrodt, F., Winter, M., Aćić, S., Agrillo, E., Alvarez, M., Ambarlı, D., Angelini, P., Apostolova, I., Arfin Khan, M.A.S., Arnst, E., Attorre, F., Baraloto, C., Beckmann, M., Berg, C., Bergeron, Y., Bergmeier, E., Bjorkman, A.D., Bondareva, V., Borchardt, P., Botta-Dukát, Z., Boyle, B., Breen, A., Brisse, H., Byun, C., Cabido, M.R., Casella, L., Cayuela, L., Černý, T., Chepinoga, V., Csiky, J., Curran, M., Ćušterevska, R., Dajić Stevanović, Z., De Bie, E., de Ruffray, P., De Sanctis, M., Dimopoulos, P., Dressler, S., Ejrnæs, R., El-Sheikh, M.A.E.M., Enquist, B., Ewald, J., Fagúndez, J., Finckh, M., Font, X., Forey, E., Fotiadis, G., García-Mijangos, I., Gasper, A.L., Golub, V., Gutierrez, A.G., Hatim, M.Z., He, T., Higuchi, P., Holubová, D., Hölzel, N., Homeier, J., Indreica, A., Işık Gürsoy, D., Jansen, S., Janssen, J., Jedrzejek, B., Jirousek, M., Jürgens, N., Kącki, Z., Kavgacı, A., Kearsley, E., Kessler, M., Knollová, I., Kolomiychuk, V., Korolyuk, A., Kozhevnikova, M., Kozub, Ł., Krstonošić, D., Kühl, H., Kühn, I., Kuzemko, A., Küzmič, F., Landucci, F., Lee, M.T., Levesley, A., Li, C., Liu, H., Lopez-Gonzalez, G., Lysenko, T., Macanović, A., Mahdavi, P., Manning, P., Marcenò, C., Martynenko, V., Mencuccini, M., Minden, V., Moeslund, J.E., Moretti, M., Müller, J.V., Munzinger, J., Niinemets, Ü., Nobis, M., Noroozi, J., Nowak, A., Onyshchenko, V., Overbeck, G.E., Ozinga, W.A., Pauchard, A., Pedashenko, H., Peñuelas, J., Pérez-Haase, A., Peterka, T., Petřík, P., Phillips, O.L., Prokhorov, V., Rašomavičius, V., Revermann, R., Rodwell, J., Ruprecht, E., Rūsiņa, S., Samimi, C., Schaminée, J.H.J., Schmiedel, U., Šibík, J., Šilc, U., Škvorc, Ž., Smyth, A., Sop, T., Sopotlieva, D., Sparrow, B., Stančić, Z., Svenning, J., Swacha, G., Tang, Z., Tsiripidis, I., Turtureanu, P.D., Uğurlu, E., Uogintas, D., Valachovič, M., Vanselow, K.A., Vashenyak, Y., Vassilev, K., Vélez-Martin, E., Venanzoni, R., Vibrans, A.C., Violle, C., Virtanen, R., Wehrden, H., Wagner, V., Walker, D.A., Wana, D., Weiher, E., Wesche, K., Whitfeld, T., Willner, W., Wiser, S., Wohlgemuth, T., Yamalov, S., Zizka, G., Zverev, A., 2019. sPlot – a new tool for global vegetation analyses. J. Veg. Sci. 30, 161–186. https://doi.org/10.1111/jvs.12710.

Butler, E.E., Datta, A., Flores-Moreno, H., Chen, M., Wythers, K.R., Fazayeli, F., Banerjee, A., Atkin, O.K., Kattge, J., Amiaud, B., Blonder, B., Boenisch, G., Bond-Lamberty, B., Brown, K.A., Byun, C., Campetella, G., Cerabolini, B.E.L., Cornelissen, J.H.C., Craine, J.M., Craven, D., de Vries, F.T., Díaz, S., Domingues, T. F., Forey, E., González-Melo, A., Gross, N., Han, W., Hattingh, W.N., Hickler, T., Jansen, S., Kramer, K., Kraft, N.J.B., Kurokawa, H., Laughlin, D.C., Meir, P., Minden, V., Niinemets, Ü., Onoda, Y., Peñuelas, J., Read, Q., Sack, L., Schamp, B., Soudzilovskaia, N.A., Spasojevic, M.J., Sosinski, E., Thornton, P.E., Valladares, F., van Bodegom, P.M., Williams, M., Wirth, C., Reich, P.B., 2017. Mapping local and global variability in plant trait distributions. Proc. Natl. Acad. Sci. 114, E10937–E10946. https://doi.org/10.1073/pnas.1708984114.

Chlus, A., Townsend, P.A., 2022. Characterizing seasonal variation in foliar biochemistry with airborne imaging spectroscopy. Remote Sens. Environ. 275, 113023.

Congalton, R.G., Gu, J., Yadav, K., Thenkabail, P., Ozdogan, M., 2014. Global land cover mapping: a review and uncertainty analysis. Remote Sens. 6, 12070–12093.

Croft, H., Chen, J.M., Wang, R., Mo, G., Luo, S., Luo, X., He, L., Gonsamo, A., Arabian, J., Zhang, Y., Simic-Milas, A., Noland, T.L., He, Y., Homolová, L., Malenovský, Z., Yi, Q., Beringer, J., Amiri, R., Hutley, L., Arellano, P., Stahl, C., Bonal, D., 2020. The global distribution of leaf chlorophyll content. Remote Sens. Environ. 236, 111479 https://doi.org/10.1016/j.rse.2019.111479.

Díaz, S., Kattge, J., Cornelissen, J.H.C., Wright, I.J., Lavorel, S., Dray, S., Reu, B., Kleyer, M., Wirth, C., Colin Prentice, I., Garnier, E., Bönisch, G., Westoby, M., Poorter, H., Reich, P.B., Moles, A.T., Dickie, J., Gillison, A.N., Zanne, A.E., Chave, J., Joseph Wright, S., Sheremet'ev, S.N., Jactel, H., Baraloto, C., Cerabolini, B., Pierce, S., Shipley, B., Kirkup, D., Casanoves, F., Joswig, J.S., Günther, A., Falczuk, V., Rüger, N., Mahecha, M.D., Gorné, L.D., 2016. The global spectrum of plant form and function. Nature 529, 167–171. https://doi.org/10.1038/nature16489.

Dong, N., Dechant, B., Wang, H., Wright, I.J., Prentice, I.C., 2023. Global leaf-trait mapping based on optimality theory. Glob. Ecol. Biogeogr. https://doi.org/10.1111/geb.13680.

Féret, J.-B., Gitelson, A.A., Noble, S.D., Jacquemoud, S., 2017. PROSPECT-D: towards modeling leaf optical properties through a complete lifecycle. Remote Sens. Environ. 193, 204–215. https://doi.org/10.1016/j.rse.2017.03.004.

Friedl, M.A., McIver, D.K., Hodges, J.C.F., Zhang, X.Y., Muchoney, D., Strahler, A.H., Woodcock, C.E., Gopal, S., Schneider, A., Cooper, A., Baccini, A., Gao, F., Schaaf, C., 2002. Global land cover mapping from MODIS: algorithms and early results. Remote Sens. Environ. 83, 287–302. https://doi.org/10.1016/S0034-4257(02)00078-0.

Fyllas, N.M., Michelaki, C., Galanidis, A., Evangelou, E., Zaragoza-Castells, J., Dimitrakopoulos, P.G., Tsadilas, C., Arianoutsou, M., Lloyd, J., 2020. Functional trait variation among and within species and plant functional types in mountainous Mediterranean forests. Front. Plant Sci. 11, 212. https://doi.org/10.3389/fpls.2020.00212.

Goll, D.S., Vuichard, N., Maignan, F., Jornet-Puig, A., Sardans, J., Violette, A., Peng, S., Sun, Y., Kvakic, M., Guimberteau, M., 2017. A representation of the phosphorus cycle for ORCHIDEE (revision 4520). Geosci. Model Dev. 10, 3745–3770.

Guerin, G.R., Gallagher, R.V., Wright, I.J., Andrew, S.C., Falster, D.S., Wenk, E., Munroe, S.E.M., Lowe, A.J., Sparrow, B., 2022. Environmental associations of abundance-weighted functional traits in Australian plant communities. Basic Appl. Ecol. 58, 98–109. https://doi.org/10.1016/j.baae.2021.11.008.

Harper, K.L., Lamarche, C., Hartley, A., Peylin, P., Ottlé, C., Bastrikov, V., San Martín, R., Bohnenstengel, S.I., Kirches, G., Boettcher, M., Shevchuk, R., Brockmann, C., Defourny, P., 2023. A 29-year time series of annual 300 m resolution plant-functional-type maps for climate models. Earth Syst. Sci. Data 15, 1465–1499. https://doi.org/10.5194/essd-15-1465-2023.

Hijmans, R.J., 2022. raster: Geographic Data Analysis and Modeling. R package version 3.5-15. R Package.

Houborg, R., McCabe, M.F., 2018. A Cubesat enabled Spatio-Temporal Enhancement Method (CESTEM) utilizing planet, Landsat and MODIS data. Remote Sens. Environ. 209, 211–226. https://doi.org/10.1016/j.rse.2018.02.067.

Hufkens, K., Bogaert, J., Dong, Q.H., Lu, L., Huang, C.L., Ma, M.G., Che, T., Li, X., Veroustraete, F., Ceulemans, R., 2008. Impacts and uncertainties of upscaling of remote-sensing data validation for a semi-arid woodland. J. Arid Environ. 72, 1490–1505. https://doi.org/10.1016/j.jaridenv.2008.02.012.

Jacquemoud, S., Ustin, S.L., Verdebout, J., Schmuck, G., Andreoli, G., Hosgood, B., 1996. Estimating leaf biochemistry using the PROSPECT leaf optical properties model. Remote Sens. Environ. 56, 194–202.

Kambach, S., Sabatini, F.M., Attorre, F., Biurrun, I., Boenisch, G., Bonari, G., Čarni, A., Carranza, M.L., Chiarucci, A., Chytrý, M., Dengler, J., Garbolino, E., Golub, V., Güler, B., Jandt, U., Jansen, J., Jašková, A., Jiménez-Alfaro, B., Karger, D.N., Kattge, J., Knollová, I., Midolo, G., Moeslund, J.E., Pielech, R., Rašomavičius, V., Rūsiņa, S., Šibík, J., Stančić, Z., Stanisci, A., Svenning, J.-C., Yamalov, S., Zimmermann, N.E., Bruelheide, H., 2023. Climate-trait relationships exhibit strong habitat specificity in plant communities across Europe. Nat. Commun. 14, 712. https://doi.org/10.1038/s41467-023-36240-6.

Kattge, J., Knorr, W., Raddatz, T., Wirth, C., 2009. Quantifying photosynthetic capacity and its relationship to leaf nitrogen content for global-scale terrestrial biosphere models. Glob. Chang. Biol. 15, 976–991. https://doi.org/10.1111/j.1365-2486.2008.01744.x.

Kattge, J., DíAz, S., Lavorel, S., Prentice, I.C., Leadley, P., BöNisch, G., Garnier, E., Westoby, M., Reich, P.B., Wright, I.J., Cornelissen, J.H.C., Violle, C., Harrison, S.P., Van Bodegom, P.M., Reichstein, M., Enquist, B.J., Soudzilovskaia, N.A., Ackerly, D. D., Anand, M., Atkin, O., Bahn, M., Baker, T.R., Baldocchi, D., Bekker, R., Blanco, C. C., Blonder, B., Bond, W.J., Bradstock, R., Bunker, D.E., Casanoves, F., Cavender-Bares, J., Chambers, J.Q., Chapin Iii, F.S., Chave, J., Coomes, D., Cornwell, W.K., Craine, J.M., Dobrin, B.H., Duarte, L., Durka, W., Elser, J., Esser, G., Estiarte, M., Fagan, W.F., Fang, J., FernáNdez-MéNdez, F., Fidelis, A., Finegan, B., Flores, O., Ford, H., Frank, D., Freschet, G.T., Fyllas, N.M., Gallagher, R.V., Green, W.A., Gutierrez, A.G., Hickler, T., Higgins, S.I., Hodgson, J.G., Jalili, A., Jansen, S., Joly, C. A., Kerkhoff, A.J., Kirkup, D., Kitajima, K., Kleyer, M., Klotz, S., Knops, J.M.H., Kramer, K., KüHn, I., Kurokawa, H., Laughlin, D., Lee, T.D., Leishman, M., Lens, F., Lenz, T., Lewis, S.L., Lloyd, J., Llusià, J., Louault, F., Ma, S., Mahecha, M.D., Manning, P., Massad, T., Medlyn, B.E., Messier, J., Moles, A.T., MüLler, S.C., Nadrowski, K., Naeem, S., Niinemets, Ü., NöLlert, S., NüSke, A., Ogaya, R., Oleksyn, J., Onipchenko, V.G., Onoda, Y., OrdoñEz, J., Overbeck, G., Ozinga, W.A., PatiñO, S., Paula, S., Pausas, J.G., PeñUelas, J., Phillips, O.L., Pillar, V., Poorter, H., Poorter, L., Poschlod, P., Prinzing, A., Proulx, R., Rammig, A., Reinsch, S., Reu, B., Sack, L., Salgado-Negret, B., Sardans, J., Shiodera, S., Shipley, B., Siefert, A., Sosinski, E., Soussana, J.-F., Swaine, E., Swenson, N., Thompson, K., Thornton, P., Waldram, M., Weiher, E., White, M., White, S., Wright, S.J., Yguel, B., Zaehle, S., Zanne, A.E., Wirth, C., 2011. TRY - a global database of plant traits. Glob. Chang. Biol. 17, 2905–2935. https://doi.org/10.1111/j.1365-2486.2011.02451.x.

Kattge, J., Bönisch, G., Díaz, S., Lavorel, S., Prentice, I.C., Leadley, P., Tautenhahn, S., Werner, G.D., Aakala, T., Abedi, M., 2020. TRY plant trait database–enhanced coverage and open access. Glob. Chang. Biol. 26, 119–188.

Kokaly, R.F., 2001. Investigating a physical basis for spectroscopic estimates of leaf nitrogen concentration. Remote Sens. Environ. 75, 153–161.

Kokaly, R.F., Skidmore, A.K., 2015. Plant phenolics and absorption features in vegetation reflectance spectra near 1.66 μm. Int. J. Appl. Earth Obs. Geoinf. 43, 55–83. https://doi.org/10.1016/j.jag.2015.01.010.

Lang, N., Kalischek, N., Armston, J., Schindler, K., Dubayah, R., Wegner, J.D., 2022. Global canopy height regression and uncertainty estimation from GEDI LIDAR waveforms with deep ensembles. Remote Sens. Environ. 268, 112760 https://doi.org/10.1016/j.rse.2021.112760.

Liu, S., Wang, Z., Lin, Z., Zhao, Y., Yan, Z., Zhang, K., Visser, M., Townsend, P.A., Wu, J., 2024. Spectra-phenology integration for high-resolution, accurate, and scalable mapping of foliar functional traits using time-series Sentinel-2 data. Remote Sens. Environ. 305, 114082 https://doi.org/10.1016/j.rse.2024.114082.

Loozen, Y., Rebel, K.T., de Jong, S.M., Lu, M., Ollinger, S.V., Wassen, M.J., Karssenberg, D., 2020. Mapping canopy nitrogen in European forests using remote sensing and environmental variables with the random forests method. Remote Sens. Environ. 247, 111933 https://doi.org/10.1016/j.rse.2020.111933.

Loveland, T.R., Belward, A.S., 1997. The IGBP-DIS global 1km land cover data set, DISCover: first results. Int. J. Remote Sens. 18, 3289–3295. https://doi.org/10.1080/014311697217099.

Macander, M.J., Nelson, P.R., Nawrocki, T.W., Frost, G.V., Orndahl, K.M., Palm, E.C., Wells, A.F., Goetz, S.J., 2022. Time-series maps reveal widespread change in plant functional type cover across Arctic and boreal Alaska and Yukon. Environ. Res. Lett. 17, 054042 https://doi.org/10.1088/1748-9326/ac6965.

Madani, N., Kimball, J.S., Ballantyne, A.P., Affleck, D.L.R., van Bodegom, P.M., Reich, P. B., Kattge, J., Sala, A., Nazeri, M., Jones, M.O., Zhao, M., Running, S.W., 2018. Future global productivity will be affected by plant trait response to climate. Sci. Rep. 8, 2870. https://doi.org/10.1038/s41598-018-21172-9.

Meyer, H., Pebesma, E., 2021. Predicting into unknown space? Estimating the area of applicability of spatial prediction models. Methods Ecol. Evol. 12, 1620–1633. https://doi.org/10.1111/2041-210X.13650.

Miller, C.E., Griffith, P.C., Goetz, S.J., Hoy, E.E., Pinto, N., McCubbin, I.B., Thorpe, A.K., Hofton, M., Hodkinson, D., Hansen, C., Woods, J., Larson, E., Kasischke, E.S., Margolis, H.A., 2019. An overview of ABoVE airborne campaign data acquisitions and science opportunities. Environ. Res. Lett. 14, 080201 https://doi.org/10.1088/1748-9326/ab0d44.

Moreno-Martínez, Á., Camps-Valls, G., Kattge, J., Robinson, N., Reichstein, M., van Bodegom, P., Kramer, K., Cornelissen, J.H.C., Reich, P., Bahn, M., Niinemets, Ü., Peñuelas, J., Craine, J.M., Cerabolini, B.E.L., Minden, V., Laughlin, D.C., Sack, L., Allred, B., Baraloto, C., Byun, C., Soudzilovskaia, N.A., Running, S.W., 2018. A methodology to derive global maps of leaf traits using remote sensing and climate data. Remote Sens. Environ. 218, 69–88. https://doi.org/10.1016/j.rse.2018.09.006.

Mugabowindekwe, M., Brandt, M., Chave, J., Reiner, F., Skole, D.L., Kariryaa, A., Igel, C., Hiernaux, P., Ciais, P., Mertz, O., 2022. Nation-wide mapping of tree-level aboveground carbon stocks in Rwanda. Nat. Clim. Chang. 1–7.

Musavi, T., Mahecha, M.D., Migliavacca, M., Reichstein, M., Van De Weg, M.J., Van Bodegom, P.M., Bahn, M., Wirth, C., Reich, P.B., Schrodt, F., Kattge, J., 2015. The imprint of plants on ecosystem functioning: a data-driven approach. Int. J. Appl. Earth Obs. Geoinf. 43, 119–131. https://doi.org/10.1016/j.jag.2015.05.009.

Ploton, P., Mortier, F., Réjou-Méchain, M., Barbier, N., Picard, N., Rossi, V., Dormann, C., Cornu, G., Viennois, G., Bayol, N., Lyapustin, A., Gourlet-Fleury, S., Pélissier, R., 2020. Spatial validation reveals poor predictive performance of large-scale ecological mapping models. Nat. Commun. 11, 4540. https://doi.org/10.1038/s41467-020-18321-y.

Potapov, P., Li, X., Hernandez-Serna, A., Tyukavina, A., Hansen, M.C., Kommareddy, A., Pickens, A., Turubanova, S., Tang, H., Silva, C.E., Armston, J., Dubayah, R., Blair, J. B., Hofton, M., 2021. Mapping global forest canopy height through integration of GEDI and Landsat data. Remote Sens. Environ. 253, 112165 https://doi.org/10.1016/j.rse.2020.112165.

Poulter, B., MacBean, N., Hartley, A., Khlystova, I., Arino, O., Betts, R., Bontemps, S., Boettcher, M., Brockmann, C., Defourny, P., Hagemann, S., Herold, M., Kirches, G., Lamarche, C., Lederer, D., Ottlé, C., Peters, M., Peylin, P., 2015. Plant functional type classification for earth system models: results from the European Space Agency's Land Cover Climate Change Initiative. Geosci. Model Dev. 8, 2315–2328. https://doi.org/10.5194/gmd-8-2315-2015.

R Core Team, 2012. R: A Language and Environment for Statistical Computing. R Foundation for Statistical Computing, Vienna.

Reich, P.B., 2014. The world-wide 'fast-slow' plant economics spectrum: a traits manifesto. J. Ecol. 102, 275–301. https://doi.org/10.1111/1365-2745.12211.

Reich, P.B., Wright, I.J., Lusk, C.H., 2007. Predicting Leaf physiology from simple plant and climate attributes: a global glopnet analysis. Ecol. Appl. 17, 1982–1988. https://doi.org/10.1890/06-1803.1.

Sabatini, F.M., Lenoir, J., Hattab, T., Arnst, E.A., Chytrý, M., Dengler, J., Ruffray, P.D., Hennekens, S.M., Jandt, U., Jansen, F., Jiménez, B., Kattge, J., Levesley, A., Pillar, V. D., Purschke, O., Sandel, B., Sultana, F., Aavik, T., Aćić, S., Acosta, A.T.R., Agrillo, E., Alvarez, M., Apostolova, I., Aubin, I., Banerjee, A., Bauters, M., Bergeron, Y., Bergmeier, E., Biurrun, I., Bjorkman, A.D., Bonari, G., Bondareva, V., Brunet, J., Čarni, A., Casella, L., Cayuela, L., Černý, T., Chepinoga, V., Csiky, J., Ćuśterevska, R., Bie, E.D., de Gasper, A.L., Sanctis, M.D., Dimopoulos, P., Dolezal, J., Dziuba, T., El, M.A., El, R.M., Enquist, B., Ewald, J., Fazayeli, F., Field, R., Finckh, M., Gachet, S., Galán, A., Garbolino, E., Gholizadeh, H., Giorgis, M., Golub, V., Alsos, I. G., Grytnes, A., Guerin, G.R., Gutiérrez, A.G., Haider, S., Hatim, M.Z., Hérault, B., Mendoza, G.H., Hölzel, N., Homeier, J., Hubau, W., Indreica, A., Janssen, J.A.M., Jedrzejek, B., Jentsch, A., Jürgens, N., Kącki, Z., Kapfer, J., Karger, D.N., Kavgacı, A., Kearsley, E., Kessler, M., Khanina, L., Killeen, T., Korolyuk, A., Kreft, H., Kühl, H.S., Kuzemko, A., Landucci, F., Lengyel, A., Lens, F., Lingner, D.V., Liu, H., Lysenko, T., Mahecha, M.D., Marcenò, C., Martynenko, V., Moeslund, J.E., Mendoza, A.M., 2021. sPlotOpen – an environmentally balanced, open-access, global dataset of vegetation plots. Glob. Ecol. Biogeogr. 00, 1–25. https://doi.org/10.1111/geb.13346.

Scheiter, S., Langan, L., Higgins, S.I., 2013. Next-generation dynamic global vegetation models: learning from community ecology. New Phytol. 198, 957–969.

Schiller, C., Schmidtlein, S., Boonman, C., Moreno-Martínez, A., Kattenborn, T., 2021. Deep learning and citizen science enable automated plant trait predictions from photographs. Sci. Rep. 11, 16395. https://doi.org/10.1038/s41598-021-95616-0.

Sellers, P.J., Hall, F.G., Kelly, R.D., Black, A., Baldocchi, D., Berry, J., Ryan, M., Ranson, K.J., Crill, P.M., Lettenmaier, D.P., Margolis, H., Cihlar, J., Newcomer, J., Fitzjarrald, D., Jarvis, P.G., Gower, S.T., Halliwell, D., Williams, D., Goodison, B., Wickland, D.E., Guertin, F.E., 1997. BOREAS in 1997: experiment overview, scientific results, and future directions. J. Geophys. Res.-Atmos. 102, 28731–28769. https://doi.org/10.1029/97JD03300.

Shi, Y., Wang, J., Qin, J., Qu, Y., 2015. An upscaling algorithm to obtain the representative ground truth of LAI time series in heterogeneous land surface. Remote Sens. 7, 12887–12908. https://doi.org/10.3390/rs71012887.

Simard, M., Pinto, N., Fisher, J.B., Baccini, A., 2011. Mapping forest canopy height globally with spaceborne lidar. J. Geophys. Res. 116, G04021. https://doi.org/10.1029/2011JG001708.

Šímová, I., Violle, C., Svenning, J.-C., Kattge, J., Engemann, K., Sandel, B., Peet, R.K., Wiser, S.K., Blonder, B., McGill, B.J., Boyle, B., Morueta-Holme, N., Kraft, N.J.B., van Bodegom, P.M., Gutiérrez, A.G., Bahn, M., Ozinga, W.A., Tószögyová, A., Enquist, B. J., 2018. Spatial patterns and climate relationships of major plant traits in the New World differ between woody and herbaceous species. J. Biogeogr. 45, 895–916. https://doi.org/10.1111/jbi.13171.

Swenson, N.G., Weiser, M.D., 2010. Plant geography upon the basis of functional traits: an example from eastern North American trees. Ecology 91, 2234–2241. https://doi.org/10.1890/09-1743.1.

Tagliabue, G., Panigada, C., Dechant, B., Baret, F., Cogliati, S., Colombo, R., Migliavacca, M., Rademske, P., Schickling, A., Schüttemeyer, D., Verrelst, J., Rascher, U., Ryu, Y., Rossini, M., 2019. Exploring the spatial relationship between airborne-derived red and far-red sun-induced fluorescence and process-based GPP estimates in a forest ecosystem. Remote Sens. Environ. 231, 111272 https://doi.org/10.1016/j.rse.2019.111272.

Thum, T., Caldararu, S., Engel, J., Kern, M., Pallandt, M., Schnur, R., Yu, L., Zaehle, S., 2019. A new model of the coupled carbon, nitrogen, and phosphorus cycles in the terrestrial biosphere (QUINCY v1. 0; revision 1996). Geosci. Model Dev. 12, 4781–4802.

Van Bodegom, P.M., Douma, J.C., Witte, J.P.M., Ordoñez, J.C., Bartholomeus, R.P., Aerts, R., 2012. Going beyond limitations of plant functional types when predicting global ecosystem-atmosphere fluxes: exploring the merits of traits-based approaches: merits of traits-based vegetation modelling. Glob. Ecol. Biogeogr. 21, 625–636. https://doi.org/10.1111/j.1466-8238.2011.00717.x.

Vallicrosa, H., Sardans, J., Janssens, I.A., Penuelas, J., 2022. Global maps and factors driving forest foliar elemental composition: the importance of evolutionary legacy. New Phytol 233, 169–181. https://doi.org/10.1111/nph.17771.

van Bodegom, P.M., Douma, J.C., Verheijen, L.M., 2014. A fully traits-based approach to modeling global vegetation distribution. Proc. Natl. Acad. Sci. 111, 13733–13738. https://doi.org/10.1073/pnas.1304551110.

Verrelst, J., Camps-Valls, G., Muñoz-Marí, J., Rivera, J.P., Veroustraete, F., Clevers, J.G. P.W., Moreno, J., 2015. Optical remote sensing and the retrieval of terrestrial vegetation bio-geophysical properties – a review. ISPRS J. Photogramm. Remote Sens. 108, 273–290. https://doi.org/10.1016/j.isprsjprs.2015.05.005.

Walker, A.P., Beckerman, A.P., Gu, L., Kattge, J., Cernusak, L.A., Domingues, T.F., Scales, J.C., Wohlfahrt, G., Wullschleger, S.D., Woodward, F.I., 2014. The relationship of leaf photosynthetic traits - V_{cmax} and J_{max} - to leaf nitrogen, leaf phosphorus, and specific leaf area: a meta-analysis and modeling study. Ecol. Evol. 4, 3218–3235. https://doi.org/10.1002/ece3.1173.

Walker, A.P., Quaife, T., van Bodegom, P.M., De Kauwe, M.G., Keenan, T.F., Joiner, J., Lomas, M.R., MacBean, N., Xu, C., Yang, X., Woodward, F.I., 2017. The impact of alternative trait-scaling hypotheses for the maximum photosynthetic carboxylation rate (V_{cmax}) on global gross primary production. New Phytol. 215, 1370–1386. https://doi.org/10.1111/nph.14623.

Wan, L., Ryu, Y., Dechant, B., Lee, J., Zhong, Z., Feng, H., 2024. Improving retrieval of leaf chlorophyll content from Sentinel-2 and Landsat-7/8 imagery by correcting for canopy structural effects. Remote Sens. Environ. 304, 114048 https://doi.org/10.1016/j.rse.2024.114048.

Wang, Y., Li, G., Ding, J., Guo, Z., Tang, S., Wang, C., Huang, Q., Liu, R., Chen, J.M., 2016. A combined GLAS and MODIS estimation of the global distribution of mean forest canopy height. Remote Sens. Environ. 174, 24–43. https://doi.org/10.1016/j.rse.2015.12.005.

Wang, L., Arora, V.K., Bartlett, P., Chan, E., Curasi, S.R., 2022a. Mapping of ESA-CCI land cover data to plant functional types for use in the CLASSIC land model (preprint). Biogeochem. Model. Terres. https://doi.org/10.5194/egusphere-2022-923.

Wang, R., Li, M., Xu, L., Li, S., He, N., 2022b. Scaling-up methods influence on the spatial variation in plant community traits: evidence based on leaf nitrogen content. J. Geophys. Res. Biogeosci. 127 e2021JG006653.

Wang, W., Fan, Y., Li, Y., Li, X., Tang, S., 2023. An individual tree segmentation method from mobile mapping point clouds based on improved 3D morphological analysis. IEEE J. Sel. Top. Appl. Earth Obs. Remote 16, 2777–2790. https://doi.org/10.1109/JSTARS.2023.3243283.

Wolf, S., Mahecha, M.D., Sabatini, F.M., Wirth, C., Bruelheide, H., Kattge, J., Moreno Martínez, Á., Mora, K., Kattenborn, T., 2022. Citizen science plant observations encode global trait patterns. Nat. Ecol. Evol. https://doi.org/10.1038/s41559-022-01904-x.

Wright, I.J., Reich, P.B., Westoby, M., Ackerly, D.D., Baruch, Z., Bongers, F., Cavender-Bares, J., Chapin, T., Cornelissen, J.H.C., Diemer, M., Flexas, J., Garnier, E., Groom, P.K., Gulias, J., Hikosaka, K., Lamont, B.B., Lee, T., Lee, W., Lusk, C., Midgley, J.J., Navas, M.-L., 2004. The worldwide leaf economics spectrum. Nature 428, 7.

Wright, I.J., Reich, P.B., Cornelissen, J.H.C., Falster, D.S., Garnier, E., Hikosaka, K., Lamont, B.B., Lee, W., Oleksyn, J., Osada, N., Poorter, H., Villar, R., Warton, D.I., Westoby, M., 2005. Assessing the generality of global leaf trait relationships. New Phytol. 166, 485–496. https://doi.org/10.1111/j.1469-8137.2005.01349.x.

Xu, M., Liu, R., Chen, J.M., Liu, Y., Wolanin, A., Croft, H., He, L., Shang, R., Ju, W., Zhang, Y., He, Y., Wang, R., 2022. A 21-year time series of global leaf chlorophyll content maps from MODIS imagery. IEEE Trans. Geosci. Remote Sens. 60, 1–13. https://doi.org/10.1109/TGRS.2022.3204185.

Yu, W., Li, J., Liu, Q., Zeng, Y., Zhao, J., Xu, B., Yin, G., 2018. Global land cover heterogeneity characteristics at moderate resolution for mixed pixel modeling and inversion. Remote Sens. 10, 856. https://doi.org/10.3390/rs10060856.

Zaehle, S., Friend, A.D., 2010. Carbon and nitrogen cycle dynamics in the O-CN land surface model: 1. Model description, site-scale evaluation, and sensitivity to parameter estimates. Glob. Biogeochem. Cycles 24.

Zhang, Y.-W., Guo, Y., Tang, Z., Feng, Y., Zhu, X., Xu, W., Bai, Y., Zhou, G., Xie, Z., Fang, J., 2021. Patterns of nitrogen and phosphorus pools in terrestrial ecosystems in China. Earth Syst. Sci. Data 13, 5337–5351. https://doi.org/10.5194/essd-13-5337-2021.

Zhang, X., Zhao, T., Xu, H., Liu, W., Wang, J., Chen, X., Liu, L., 2024. GLC_FCS30D: the first global 30 m land-cover dynamics monitoring product with a fine classification system for the period from 1985 to 2022 generated using dense-time-series Landsat imagery and the continuous change-detection method. Earth Syst. Sci. Data 16, 1353–1381. https://doi.org/10.5194/essd-16-1353-2024.